Department of Precision and Microsystems Engineering

Air loading on ultrathin graphene membranes for microphone application

C. van Ruiten

Report no : 2023.017
Coach : Prof.dr. P.G. (Peter) Steeneken
Professor : Prof.dr. P.G. (Peter) Steeneken
Specialisation : Dynamics of Micro and Nanosystems
Type of report : Master Thesis
Date : March 31, 2023

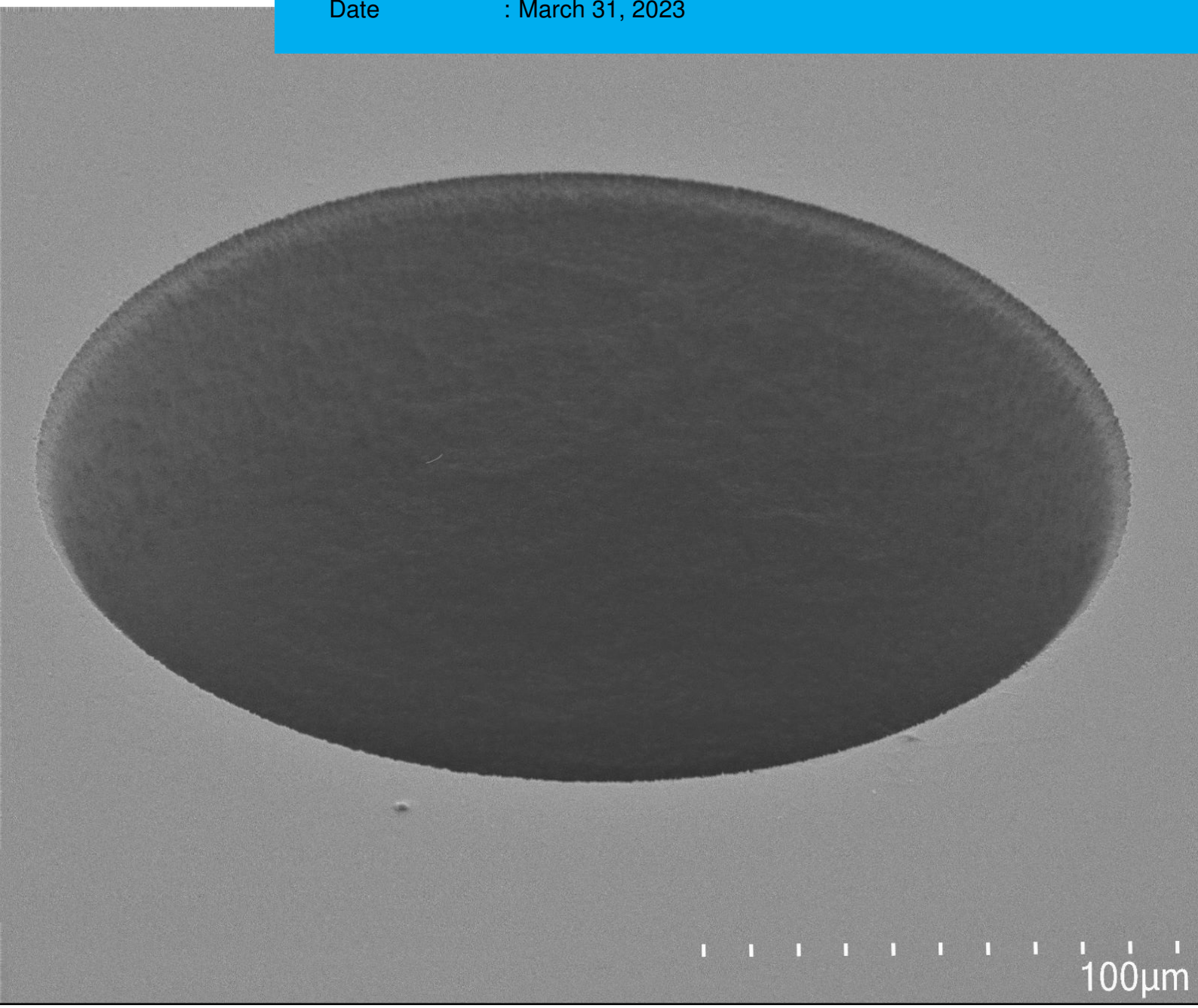

Air loading on ultrathin graphene membranes for microphone application

by

Cas van Ruiten

to obtain the degree of Master of Science
at the Delft University of Technology,
to be defended publicly on Friday March 31, 2023 at 1:00 PM.

Student number:	4565304	
Project duration:	November 1, 2021 – March 31, 2023	
Thesis committee:	Prof. dr. Prof.dr. P.G. Steeneken,	TU Delft, supervisor
	R. Pezone,	TU Delft, supervisor
	Dr. G.J. Verbiest,	TU Delft

TU Delft

Contents

Abstract

This thesis explores the challenges of using ultrathin graphene membranes in microelectronic mechanical sensors (MEMS) technology, specifically in the development of MEMS microphones. Graphene, being only an atom thin and one of the strongest known materials, offers promising potential for further miniaturization of MEMS microphones. However, the mass loading effect on the graphene membrane can impact the device's resonance frequency and bandwidth.

To address this issue, this study analyzes the dynamic response of the graphene membrane under different pressures and membrane parameters, such as diameter and thickness.

The membranes are fabricated by using chemical vapour deposition, after which the membranes are transferred over a cavity. The measuring setup uses a laser Doppler vibrometer to measure the deflection of the membranes and investigate their dynamic response. Pressure-dependent experiments are performed to measure the resonance frequency of the membrane's response, and the relationship between the radius, thickness, and resonance frequency is explored. By doing these measurements we explore the effect of air loading to investigate the ultimate performance limits of graphene membranes for microphone application.

The experimental results show a clear presence of the air loading effect and align with earlier models of the resonance frequency with mass loading effects. The thesis validates the accuracy and reliability of the measurements and contributes to the body of knowledge surrounding the topic. The limitations of the study include fabrication imperfections and setup difficulties like a limited bandwidth of the piezo-shaker used for the actuation of the membranes. The assumptions made about limited cavity effects are also discussed. Future research could explore the impact of an added backplate with venting holes for capacitive readout. Next to that, the influence of air loading on the system's damping could be researched.

1 Introduction

Micro-electromechanical sensors (MEMS) have seen a spread in consumer electronics due to their reduction in size, power consumption, and unit costs. The ever-continuing trend to downscale these devices contains many new challenges. These technological improvements and size reduction is desired to meet society's continuing need to enhance consumer electronics. An example of MEMS technology is the microphone. For further miniaturisation of MEMS microphones, the microphone's membrane should become thinner to reach similar sensitivities to those of larger devices. With the use of graphene, one of the strongest known materials while being only a few atoms thin, the limits of sensing capabilities are pushed. Graphene owes its strength to the strong atom-to-atom bonds present in the flat hexagonal structure.

This thesis focuses on the challenges induced by the mass loading effect on ultrathin graphene membranes for use in MEMS microphone technology. The mass loading effect results in an added virtual mass to the membrane lowering the resonance frequency and thereby decreasing the bandwidth of the device. Researching this effect is necessary to continue enhancing mechanical sensitivity while maintaining an adequate bandwidth. The analysis is done by examining the changes in the dynamic response of the membrane, most specifically the resonance frequency, over different pressures and membrane parameters such as diameter and thickness.

Starting with an introduction to graphene and the working principles of condenser microphones, wherein these sensing membranes find their application. This is followed by an in-depth study of theoretical concepts that form the foundation of this work, as well as a review of the current state of the art of graphene and microphone technology. The experimental methods are explained and the obtained results are provided. Finally, the results are discussed and conclusions are drawn.

1.1. Graphene

With a Young's modulus of over 1 TPa for monolayer graphene [1], graphene is the strongest known material ever measured [2]. After the discovery of the material, a lot of research was done on trying to use this material to increase the performance of sensors. Graphene has extraordinary mechanical properties like high yield strength, low mass density and bending rigidity, as well as electrical properties like high carrier mobility [3]. Due to these properties, a lot of progress was made to implement graphene in micro- or nano-sized devices to enhance performance or allow further miniaturization [4]. The incredible strength and flexibility with low mass and thickness makes the use of graphene promising, especially in the field of pressure-related sensors because of the possibility to achieve very high-aspect ratios [4], making them extremely sensitive to any changes in pressure in their surroundings [5]. This sensitivity to pressure changes gives potential to better performing acoustic sensors. An example of such a sensor and the focus of this thesis is the condenser microphone which converts sound waves into an electric signal via capacitive readout between the backplate and the moving membrane. Replacing the movable membrane with graphene results in a measured increase in the sensitivity [6, 7]. This is due to the lower internal stresses and larger aspect ratios of the graphene membrane.

The potential of graphene as a material for pressure-sensitive sensors is hindered by several limitations, including fabrication challenges that lead to low yields and low tension reproducibility. Addition-

ally, the presence of squeeze film damping which arises from the squeezing of a thin film of fluid inside the cavity, and a low resonance frequency within the audible range at atmospheric pressure also pose significant problems. The low resonance frequency can be explained by the effect of air loading which has an unknown but reported considerable impact on the resonance frequency for nanometer-thick membranes.

The production of single and multi-layer graphene can be done in multiple ways. Examples are chemical vapour deposition (CVD), mechanical exfoliation, liquid-phase exfoliation or the reduction of graphene oxide (GO) [4, 8]. Different methods report varying mechanical, thermal or electric properties due to slightly varying quality.

For single-layer graphene, defects have a strong influence on the electronic, optical, thermal, and mechanical properties of the lattice [9]. Multiple types of defects influence these properties. Examples of these imperfections are point defects, vacancies and adatoms in the crystal structure. These non-equilibrium defects can come from different mechanisms like crystal growth due to the process not happening atom-by-atom, therefore causing natural imperfections. It can also happen through particle irradiation with electrons or ions that can generate point defects due to the ballistic ejection of carbon atoms in the graphene [9]. Lastly, the effect of wrinkles and non-uniformities have a big influence on these suspended 2D materials [10].

In this study, multi-layer CVD-grown graphene on molybdenum as a catalyst metal is used [11]. With this method, it is easier to fabricate large membranes due to their multi-layer nature. The membranes do show imperfections resulting in changes in their mechanical properties.

1.2. Condenser MEMS microphones

An introduction of microphone and diaphragm or membrane technology is provided together with relevant microphone performance parameters. Next to that, a summary is added to map the existing MEMS microphone technology. A more in-depth study is done into the application of graphene in microphones and the limitations of the existing technologies.

A microphone is a dynamic pressure transducer made to detect sound waves over a broad range of frequencies, generally designed to have the highest performance in the human audible range (20 Hz-20 kHz) [12]. How the exact transduction is done depends on the type of microphone. Due to its good performance, low cost, and ease of manufacturing the focus in the industry has been on condenser microphones [13]. A condenser microphone works by measuring the change in the capacitance C between the movable and fixed plates. This is done by relating the potential difference V to the charge on the capacitor q by the equation:

$$C = \frac{q}{V}. \tag{1.1}$$

The capacitance of a flat capacitor in a vacuum is given by:

$$C = \epsilon_0 \frac{A}{d}. \tag{1.2}$$

The capacitance is dependent on the distance between the plates d, the area of the capacitive plate A, and the permittivity constant of free space $\epsilon_0 = 8.8542 \times 10^{-12}$ C^2/Nm^2. Combining equations 1.1 and 1.2 yields the measured voltage

$$V = q \frac{d}{A\epsilon_0}. \tag{1.3}$$

A schematic of a condenser microphone can be seen in Figure 1.1 [12]. In this schematic the sound waves displace the diaphragm (or membrane) changing the distance and thereby capacitance between the membrane and backplate. The electrical signal that is generated is amplified and processed. A bias voltage V_b is needed to provide a source of electric charge q whose magnitude directly determines the microphone sensitivity.

Key performance parameters of microphones are sensitivity, (signal to) noise levels, power consumption, resonant frequency, and size [13, 14]. How sensitive a microphone is can be described by the open circuit sensitivity. The open circuit sensitivity of a microphone is the ratio of the microphone's open circuit voltage to the sound pressure level applied to the microphone by a sound source. Open circuit sensitivity of a microphone consists of two parts: the mechanical sensitivity S_m, which is the

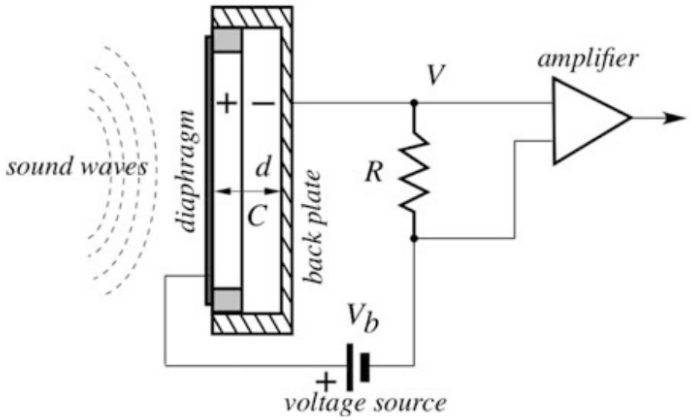

Figure 1.1: A schematic of a condenser microphone where sound waves displace the diaphragm changing the distance and thereby capacitance between the diaphragm and backplate. The electrical signal that is generated is amplified and processed. A bias voltage V_b is needed to provide a source of electric charge q [12].

change of the air gap Δg due to a change in pressure ΔP, and the electronic sensitivity S_e, which depends on the value of the bias voltage V_b and thickness of the air gap g described by the following equation [13]:

$$S = S_e \cdot S_m = \frac{V_b}{g} \cdot \frac{\Delta g}{\Delta P}. \tag{1.4}$$

The mechanical sensitivity of a membrane can be quantified using Equation 1.5 [13]. Where R is the radius and σ_0 is the stress in the membrane. The stress is composed as $\sigma_0 = n_0/h$, where n_0 is the pre-tension and h is the thickness of the membrane.

$$S_m = \frac{R^2}{8\sigma_0 h} = \frac{R^2}{8n_0}. \tag{1.5}$$

With the basic working principles and performance parameters of a condenser microphone covered, the next section will introduce the theoretic concepts that form the foundation of this thesis. Furthermore, some of the research done in implementing graphene to increase the performance of pressure sensors including microphones is provided.

2

Theory and literature review

In this chapter, a short introduction to some general concepts is given that form the groundwork of this thesis. Next to that, the state of the art of MEMS microphones is given in an overview.

2.1. Membrane dynamics

With the growing importance of suspended two-dimensional materials in sensor applications, multiple kinds of research with different actuation types and materials were conducted to study the dynamical behavior of these atomically thin layers [5]. Understanding the dynamics of these membranes is important to further characterize the membranes in linear or nonlinear regimes. In Figure 2.1 a schematic overview is shown with relevant membrane parameters.

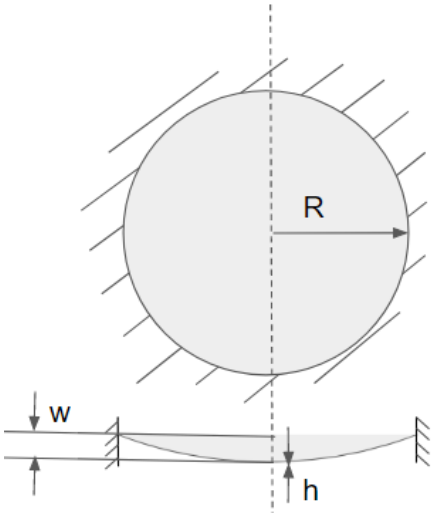

Figure 2.1: A schematic figure of a clamped membrane, where R is the radius, w is the out-of-plane displacement and h is the thickness of the membrane.

In particular, for microphone applications, the sensor's performance is determined by the membrane's displacement under sound pressure. For small out-of-plane action, the in-plane displacements can be neglected. The out-of-plane displacement function can be written as $w(x, y, t)$. Deriving from mechanics, this motion can be rewritten in terms of linear eigenmodes $\phi_i(x, y)$ and the generalized coordinates $q_i(t)$ as $w(x, y, t) = \Sigma_i^N q_i(t)\phi_i(x, y)$.

For a very thin circular membrane, the pre-tension n_0 dominates the restoring force. With the assumption that the pre-tension is uniform over the surface, the out-of-plane deflection w can be written in the cylindrical coordinates R and θ and with the use of the density ρ and thickness h of the membrane this results into the following equation of motion [5]

$$\frac{\partial^2 w}{\partial R^2} + \frac{1}{R^2}\frac{\partial^2 w}{\partial \theta^2} + \frac{1}{R}\frac{\partial w}{\partial R} = \frac{\rho h}{n_0}\frac{\partial^2 w}{\partial t^2}. \tag{2.1}$$

A solution to this formula yields the fundamental resonance frequency f_0 which can be calculated with Equation 2.2 [5]. More on resonance frequency in Section 2.1.1.

$$f_0 = \frac{2.405}{2\pi R}\sqrt{\frac{n_0}{\rho h}}. \tag{2.2}$$

As a first approximation, a microphone membrane is a harmonic oscillator driven by changes in pressure due to sound waves. The harmonic oscillator model shown in Figure 2.2 illustrates why the resonance frequency is important to reach a high bandwidth, as a steep decline in performance can be observed for frequencies above the resonance frequency. For microphone application, a resonance frequency outside the audible range ($f_0 > 20$ kHz) is desired to achieve a bandwidth that is sufficiently large to capture all audible frequencies.

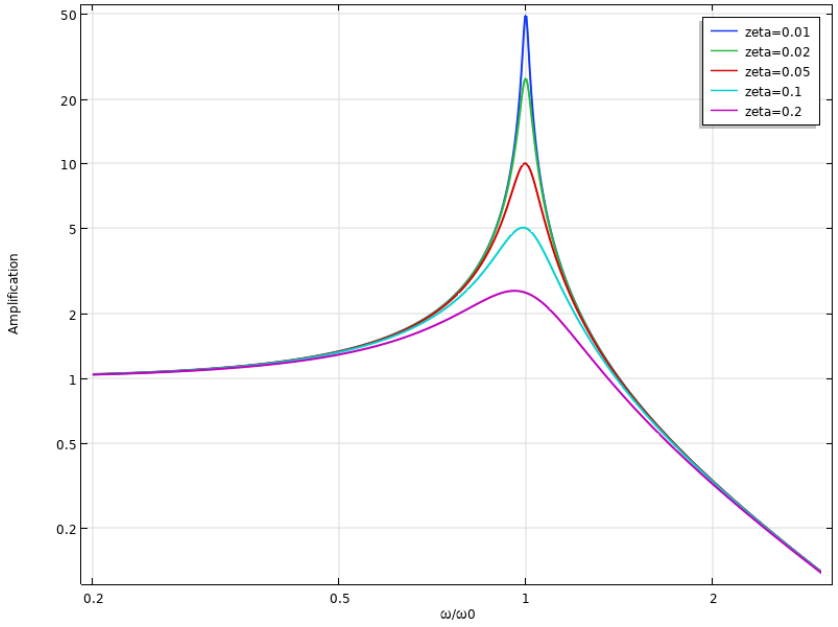

Figure 2.2: Example bode plot of the normalized frequency response of a harmonic oscillator [15]. The different colours correspond to different magnitudes of damping.

With the assumption that the centre deflection of a microphone membrane is large compared to the thickness of the membrane, the relation between the pressure change ΔP and the centre deflection w can be written as [16]:

$$\Delta P = 4\frac{n_0}{R^2}w + \frac{8Eh}{3R^4(1-\nu)}w^3, \tag{2.3}$$

where E is the Young's modulus and ν the Poisson's ratio of the material.

The membrane dynamics in microphones can often be estimated with a linear response. However, it is notable that for possible large deflections of graphene microphones, the non-linear effects that occur for high amplitudes do limit the dynamic range, which is the difference between the maximum and lowest (noise floor) sound pressure level (SPL) it can properly detect [6]. The limited dynamic range due to non-linear effects becomes clear from the cubic term in Equation 2.3.

2.1.1. Resonance frequency in microphone application

As mentioned before, a good first approximation for a microphone membrane is the harmonic oscillator model. When designing a microphone, the fundamental frequency and thereby bandwidth should be

as high as possible for good performance over that range. In this thesis we assume the upper bound of the bandwidth to be similar to the resonance frequency. It is important that the membrane is designed such that all resonance modes have a resonance frequency larger than the required bandwidth of the microphone. Higher bandwidths can be reached by increasing the tension or stiffness of the membrane. A downside to increasing the tension is the decrease of the mechanical sensitivity as can be concluded from Equation 1.5. The low bandwidth of graphene membranes due to the low stiffness and large contribution of air damping is mentioned by Baglioni, G. et al (2022) [6], being close to 2-3 kHz for their membranes. This resonance frequency is well below the application range of most microphones.

Other research done on large-size graphene membranes [7, 17, 18] show a resonance frequency in the audible range too. For smaller graphene membranes (R= 20 μm) researched by Wittman, S. et al (2019) [19] the resonance frequency does go above the audible range. Showing that it is possible to have graphene membranes with a resonance frequency of over 20 kHz.

In other research on graphene membranes for microphone application [20], the resonance frequency was relatively high when measuring at lower pressures. These samples were measured at 10^{-4} kPa to reduce the air-damping effect. In the same paper, variations in the pre-tensions were said to be a possible cause for deviations between experimental and theoretical resonance frequencies. These deviations can be caused by small non-uniformities in the graphene boundary conditions due to variations in imperfect hole geometries, differences in the clamping electrode geometries or silicon di-oxide residuals between the graphene and the silicon substrate [20]. These factors show the difficulty when working with ultrathin membranes. However, with the proven improvement in sensitivity of graphene microphones, the possibility of reducing dimensions to lose some of their sensitivity as a trade-off for reaching a higher bandwidth is possible. This would allow for miniaturizing the device while still keeping a sensitivity comparable to present MEMS microphones.

2.1.2. Mode shapes

The focus of this thesis is the motion of circular membranes because of the membranes provided. We simplify the dynamic behaviour with the use of their properties in resonance. We start from the equation of free motion given in Equation 2.1. The deflection is dependent on both the radial coordinate from the centre r and the angular coordinate θ. We use the separation of the variables, T a function of the angular coordinate and τ the time-dependent component, to find a solution to this equation [21]:

$$w(r,\theta,t) = R(r)T(\theta)\tau(t). \tag{2.4}$$

We assume a harmonic vibration for the time-dependent component τ:

$$w(r,\theta,t) = R(r)T(\theta)sin(\omega t). \tag{2.5}$$

Using the separation constant $\lambda^2 = \frac{\omega^2 \rho h}{n_0}$ we can write the equation of motion as:

$$\left(R'' + \frac{1}{r}R' + \lambda^2 R\right)T + \frac{1}{r^2}R(r)T'' = 0. \tag{2.6}$$

The equation of motion can now be separated into two ordinary differential equations by using the constant m^2:

$$T'' + m^2 T = 0, \tag{2.7}$$

and

$$R'' + \frac{1}{r}R' + \left(\lambda^2 - \frac{m^2}{r^2}\right)T = 0. \tag{2.8}$$

Equation 2.7 is a harmonic equation with the general solution:

$$T(\theta) = A_{1,m}\sin(m\theta) + A_{2,m}\cos(m\theta), \tag{2.9}$$

where $m = 0, 1, 2, ...$
Equation 2.8 is a Bessel-type equation that has the general solution:

$$R(r) = J_m(\lambda r), \tag{2.10}$$

which at radius a of the membrane is:

$$J_m(\lambda a) = 0. \tag{2.11}$$

Taking $\alpha_{mn} = \lambda a$, we find infinitely many roots to this equation, the lowest being $\alpha_{01} = 2.405$. Substituting this back into the definition of the separation constant, we get

$$\omega_{mn} = \frac{\alpha_{mn}}{a}\sqrt{\frac{n_0}{\rho h}}. \tag{2.12}$$

This result is in direct correspondence with Equation 2.2. The solutions to Equation 2.1 give the resonance frequencies and eigenmodes of which the four lowest resonance mode shapes are shown in Figure 2.3 [21].

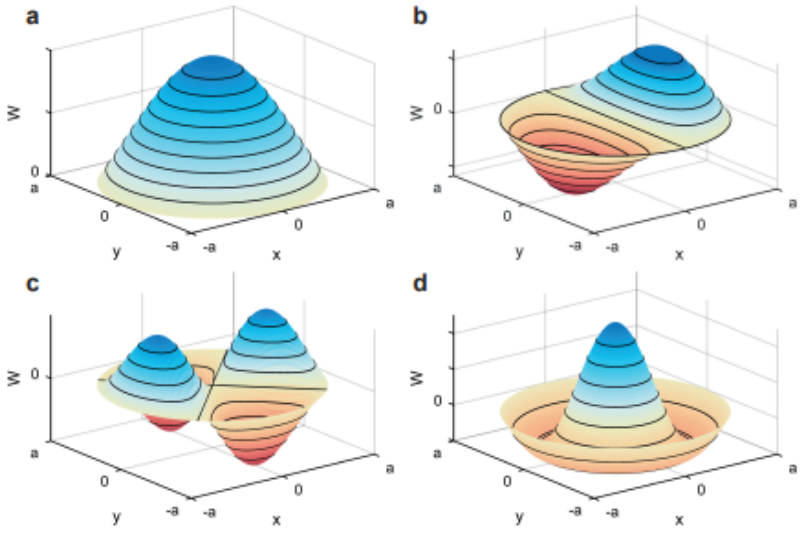

Figure 2.3: Visualization of the mode shapes with the four lowest frequencies. a) First/fundamental mode (0, 1). b) Mode (1,1). c) Mode (2,1). d) Mode (0,2) [21].

2.2. Air damping and loading

A major limitation in MEMS microphones is the interaction with air molecules around the membrane. As shown before in Equation 1.5, the sensitivity increases when decreasing the thickness or increasing the size of the membrane. These changes in dimensions have the downside of having a bigger surface area exposed to air. Next to that, the decrease of the thickness results in having lower mass and therefore impulse when moving. Since single-layer graphene is almost impermeable to gases, including helium [3], this could trap the gasses effectively in a closed cavity, leading to squeeze film effects. The squeeze film effect occurs when a thin film is compressed between two surfaces. This effect occurs in two regimes, in the first regime, which is applicable for lower frequencies, the viscous damping force is dominant. The second regime applies for higher frequencies of the membrane in which the elastic force is dominant [22]. The squeeze film effect is further elaborated on in Appendix A.1.

Additionally, microphone studies with nano to micrometre thin membranes mention a decrease in the resonance frequency due to mass loading effects [7, 23–25]. This effect appears to have a significant influence on the low-mass graphene membranes. Mass loading is the phenomenon whereby the effective mass of the object is increased because of fluid coupling between the membrane and the fluid [26]. This added mass decreases the resonance frequency according to Equation 2.2. In the case of microphones, this fluid is air and therefore the effect will be referred to as air loading in this thesis. Many

studies have been conducted to understand the behaviour of graphene membranes in high vacuum. However, due to the high vacuum, there is no medium present to cause loading effects. Since microphones are used in atmospheric conditions, the high resonance reported in vacuum by these studies for thin membranes [5, 20] is not as promising for real-world application. The 5- to 10-fold decrease in resonant frequency when changing the pressure, reported in Baglioni, G et al (2022) [6], suggests a large influence from the air loading. This effect of air loading on the membrane dominates the mass of the membrane according to some microphone studies [7, 27]. For the ultrathin graphene membranes this effect in the air might have similar problems to the reported influence of fluid loading in other studies [28]. More studies are conducted on the effects of fluid coupling on plates [29, 30].

To understand the physical origin of the mass loading effect, we use the acoustic radiation impedance on the membrane which is derived from the theory by Blackstock, D.T. [26], Bouwkamp, C.J. [31] and Morse, P.M. [32].

Let there be a periodically changing pressure field $p = Pe^{j\omega t}$ with the average pressure amplitude on the face of the membrane or piston P_{av}. The piston velocity amplitude is u_0, resulting in the radiation impedance

$$Z_p = \frac{P_{\text{av}}}{u_0} = \frac{F/\pi R^2}{u_0}, \tag{2.13}$$

where F is the total force exerted by the sound field on the piston [26]. To find F, we need to integrate the local pressure over the face of the piston,

$$F = \int P(A)dS'. \tag{2.14}$$

A is an arbitrary point on the piston, dS' is an incremental area on the piston as seen in Figure 2.4 and k is the wave number. When computing F we count the force on dS' due to the pressure at dS as well as the force on dS due to the pressure at dS'. This can be seen as the radiation of an arbitrary area on the membrane (self-)impeding another area on the membrane.

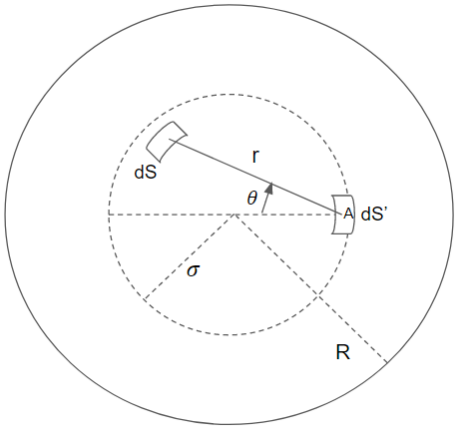

Figure 2.4: Geometry used for calculating the pressure on the membrane face (reconstructed from [26]).

To find $P(A)$, we use the Rayleigh integral, $dS = rdrd\theta$ and the theory of the radiation from a baffled piston of arbitrary shape to find

$$P(A) = \frac{jkP_0}{2\pi}\int_{-\pi/2}^{\pi/2} d\theta \int_0^{2\sigma\cos\theta} \frac{e^{-jkr}}{r} rdr, \tag{2.15}$$

where the fictitious pressure at the piston face $P_0 = \rho_0 c_0 u_0$ consisting of ρ_0 which is the density of the medium and c_0 is the speed of sound in the acoustic medium. Computing the integral steps with the use of Struve and Bessel functions similar to literature [26], we arrive at the equation

$$F = 2\pi R^2 P_0 \left[1 - \frac{2J_1(2kR)}{(2kR)} + j\frac{2K_1(2kR)}{(2kR)}\right], \tag{2.16}$$

where J_1 is the first order Bessel function and K_1 is the first order Struve function. Substituting Equation 2.16 into Equation 2.13 yields the expression for the radiation impedance of the piston

$$Z_p = \rho_0 c_0 \left[1 - \frac{2J_1(2kR)}{(2kR)} + j\frac{2K_1(2kR)}{(2kR)}\right], \tag{2.17}$$

This theory can be used to write the coupling with the acoustic domain in the simpler form $Z_p = R_r + jX_r$. The real part is the radiation resistance, which corresponds to pressure which propagates in the medium and can be seen as an additional damping to the device. The imaginary part is the radiation reactance which represents the loading effect. This can be thought of as the energy stored in the fluid that continuously reacts with the vibrating surface and impedes its motion. The stored energy in the fluid does not travel away from the radiator but adds to it. This makes the medium on the membrane act as the extra mass and reduces the resonance frequency [31]. The radiation impedance can therewith be thought of as the reaction of the air back on the membrane [33].

An important factor for the coupling between the fluid and the membrane is the added virtual mass incremental (AVMI). This factor is derived from the ratio between the reference kinetic energy of the fluid T_F, due to the vibrations, and that of the kinetic energy of the membrane or plate T_M [30]:

$$\beta = \frac{T_F}{T_M}. \tag{2.18}$$

Here, β is the AVMI factor [30, 34]. With the assumption that the mode shapes in a vacuum and in fluids are to be the same, the following relation between the resonance frequency in a vacuum, f_v, and in a fluid, f_f, is obtained:

$$f_f = \frac{f_v}{\sqrt{1+\beta}}. \tag{2.19}$$

The AVMI can be derived from the following equation:

$$\beta = \Gamma(\rho_a/\rho_g)(R/h). \tag{2.20}$$

Here, ρ_a and ρ_g are the air and graphene membrane's density, respectively, and Γ is the non-dimensionalized added virtual mass index (NAVMI) which is dependent on the geometry and clamping geometry of the membrane.

With low reported resonance frequencies and thereby bandwidth in ambient pressure, graphene microphones will not yet be viable for microphone application for the audible range. The understanding of the air loading effect for the large diameter but thin membranes to better design microphones is of high importance to have acceptable bandwidth. Combining equations 2.2, 2.19 and 2.20 gives the analytical model for the fundamental resonance frequency:

$$f_0(P) = \frac{2.405}{2\pi R}\sqrt{\frac{n_0}{\rho_g h_g + \Gamma\rho_a(P)R}}. \tag{2.21}$$

In this corrected equation, the resonance frequency is dependent on the density of the medium and thereby pressure. Therefore, the air loading effect can be investigated by changing the density of the atmospheric gas. This can be done, as further elaborated on in Section 3, by lowering the pressure which decreases the number of air molecules present or by changing the gas completely to one with a different density.

2.3. State of the art

As mentioned before, graphene has exceptional properties able to replace other materials to improve sensors by scaling down or increasing their performance. It should even inspire to investigate completely new applications and designs [4]. Examples of mechanical sensors that use graphene are microphones [7, 17, 19, 35–39], pressure sensors [16, 40, 41] and resonators [42–45].

With its high yield strength, low tension and high flexibility, the potential of graphene is successfully harvested to enhance devices by improving sensitivity or allowing for further miniaturization without performance loss. With the novelty of the technology, there are still aspects to further investigate and

reach the full potential of the material for sensor application. But it shows that graphene is a promising material to further improve mechanical sensors.

In Figure 2.5 by Woo, S. et al (2017) [17], a fully operating electret condenser microphone (ECM) is shown made from multilayer graphene and PMMA. Even though this research uses a thick membrane of around 3 µm, a big increase of 9 dB in mechanical sensitivity over their reference microphone is reported [17]. This microphone is fully self-assembled from its components.

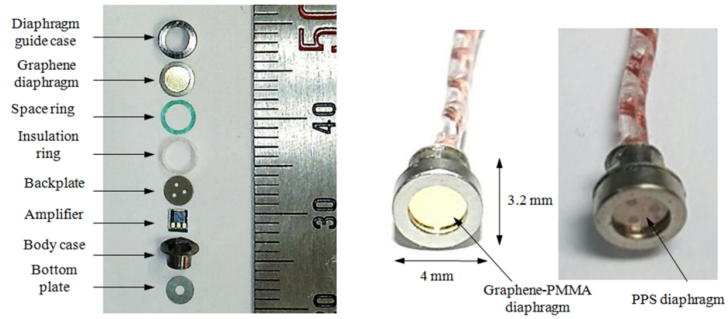

Figure 2.5: Structure and photograph of the proposed microphone and the fabricated microphone using the ECM diaphragm [17].

Further analysis is conducted on different MEMS microphones with the help of the review paper on MEMS microphones by Zawawi, S.A. et al (2020) [13]. In this paper, many MEMS microphone designs and papers are summarized and analyzed to further emphasize the different parameters and effects that are of importance for higher performing MEMS microphones.

Figure 2.6 shows a scatter plot of different MEMS microphones with their mechanical sensitivity in nanometers per Pascal plotted against the radius squared over the thickness. Trend lines can be seen indicating similar stresses on the membranes following Equation 1.5. A clear mechanical superiority can be seen for graphene MEMS microphones. This can be explained by having lower stresses and smaller thicknesses. It should be noted that the stress in the membrane is also affected by the clamping geometry [20].

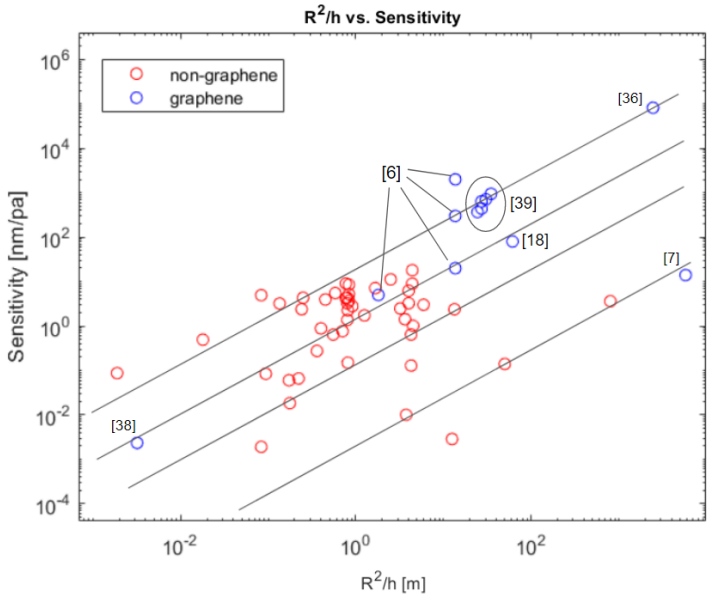

Figure 2.6: R^2/h plotted against the mechanical sensitivity in [nm/Pa] with added trend lines to show membranes with similar tension according to Equation 1.5. The higher lines have lower tension. Blue circles indicate microphones using graphene and the red circles are without graphene retrieved from [13].

Membranes in the study done by Baglioni, G et al (2022) [6], show extremely high mechanical

sensitivities displayed in Figure 2.7 compared to their reference microphone in the audible range. The low reported stress in the graphene membrane is also in agreement with the mentioned trend lines. This study however has no backplate which has an unreported effect on mechanical sensitivity compared to microphones with backplates. Next to that, the used membranes have their resonance frequencies far inside the audible range. A trade-off between the mechanical sensitivity and the resonance peak can be observed.

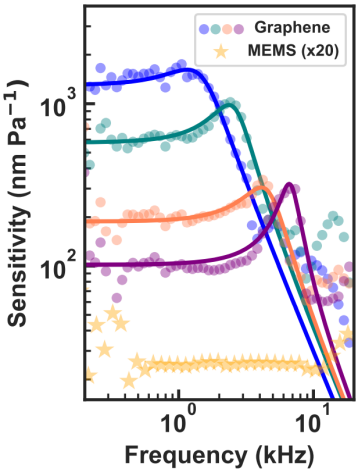

Figure 2.7: Audio response spectra of graphene membranes (R = 175 µm) and the Si membrane in the ST-M MEMS microphone. Drawn lines are fit to the data using a harmonic oscillator model [6].

Out of the many papers discussing MEMS microphone designs by Zawawi, S.A. et al (2020) [13] only five use graphene. Out of these five recent papers, two use multilayer membranes and three use only a graphene membrane as the diaphragm. Apart from these mentioned papers, more studies have been conducted on the novel technology of MEMS graphene capacitive microphones [6, 36, 39]. These papers show once again the potential that (multi-layer) graphene has for the application of microphones, having responses of -47.5 dB V (4.22 mV/Pa) [35]. Todorovic, D. et al (2015) [7] used a 25 nm thick graphene membrane to outperform a professional microphone (with a membrane thickness of the order of 1 µm) in the same packaging. This same microphone responded to a range extending to a frequency of 1 MHz. In the research of Wittmann, S. et al. [19], a graphene microphone is realized with a diameter of 40 µm that is claimed to be resonance-free up to frequencies of over 700 kHz. However, having a lower sensitivity than silicon-based microphones by a factor of 5, they mention their microphone has a clear advantage when it comes to scalability. In the study on graphene/PMMA microphones done by Xu et al. [35], 6-layer graphene and 450 nm PMMA has been dry-transferred on the silicon dioxide substrate. This way they created a microphone with a backplate with a diameter of 3.5 mm visible in Figure 2.8. However, they have an absence of mode (0, 1) which is of importance for capacitive readout to measure the largest change in capacitance between the two plates.

These papers have shown the possibility of making extremely large and thin membranes for microphone applications, which can validate the theoretically expected increase in performance.

To increase the performance of MEMS (graphene) microphones, multiple difficulties come into play. Looking at Equation 1.5, the mechanical sensitivity of a microphone can be increased by decreasing the stress in the membrane. Larger graphene membranes show improvements in lowering this stress in the membrane [20]. However, fabricating those large and low-stress graphene membranes show difficulties when transferring over a cavity.

For the extremely thin membranes, the sensitivity and frequency response is defined by the geometry and the membrane static tension [7]. While the reduction of stress in the membranes gives the mentioned increase in mechanical sensitivity, it also has downsides like the lowering of the stiffness resulting in a lower resonance frequency and decreasing the pull-in voltage which is the maximum voltage possible until stiction issues occur as further explained in Appendix A.3. With ultra-low mass membranes, the influences of air around the membrane have more significant effects than ever before. The air effects like the squeeze film effect and air loading cause a further decrease in performance. In

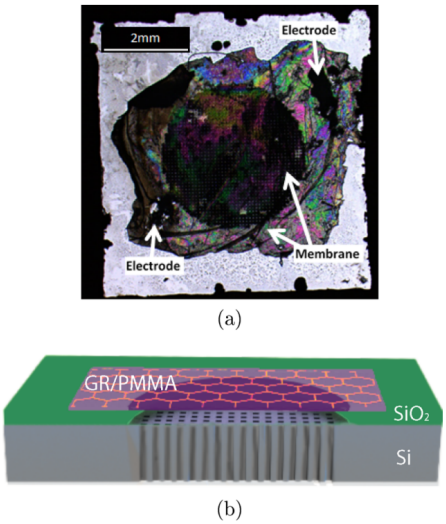

Figure 2.8: Optical microscopy image (a) and cross-section schematic (b) of the graphene-based electrostatic microphone [35].

this thesis we will study the ultimate performance limits of graphene microphones within the discussed constraints and will get back on this topic in Section 5.2.

3

Methods

This chapter describes the fabrication procedures used in this thesis to make graphene membranes over an open cavity. Next to that, the laser Doppler vibrometer setup using a vacuum chamber and piezo shaker is shown. Together they actuate and read out the motion of the membranes while being able to set the environments to different pressure. Then the different setups are mentioned which further investigate the mode shapes.

3.1. Fabrication

In this research, Chemical vapour deposition (CVD) is the method used to fabricate the membranes. CVD is often used to deposit or grow thin films and has been the workhorse of depositing materials in semiconductor devices for decades [4]. A schematic of a general CVD process can be seen in Figure 3.1.

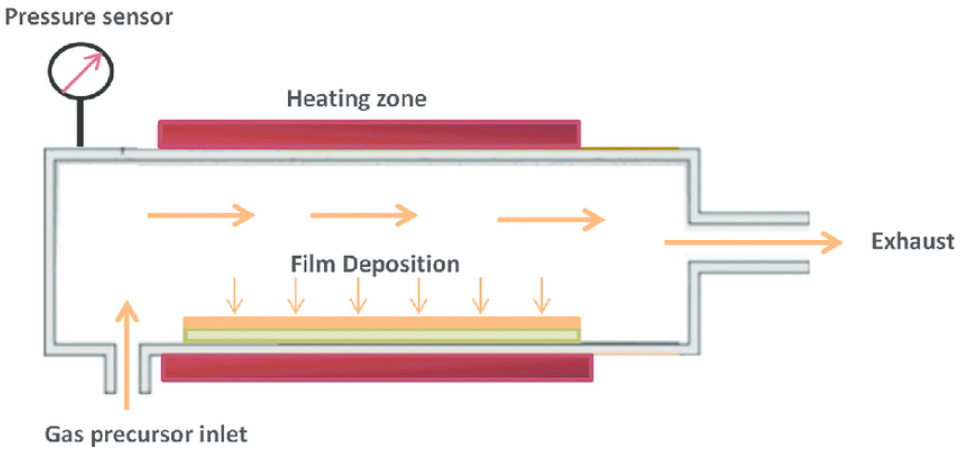

Figure 3.1: A schematic representation of a standard CVD process [46].

Fabrication of the suspended graphene structures is done by growing the graphene with CVD and afterwards transferring the membrane over an open cavity. Due to the transfer step and medium, imperfections like polymer contamination, crack formation, wrinkling, folding, delamination and low tension reproducibility may become present [20]. The free-standing membranes are made of multilayer graphene with a thickness of approximately 8 nm grown on Si/SiO_2/Mo (50 nm) by Low-Pressure Chemical Vapour Deposition in an Aixtron Black Magic reactor at 1000 °C with H_2 - CH_4 as carbon precursor source. The Mo seed layer under the graphene is wet-etched with H_2O_2 and washed in deionized water, after which the graphene remains on the Si/SiO_2 substrate. The graphene is finally immersed in DI-water until it delaminates and it is carefully wet-transferred on a Si/SiO_2 substrate (thickness of $\sim$ 520 µm) with pre-patterned holes. The transfer process is shown in Figure 3.2.

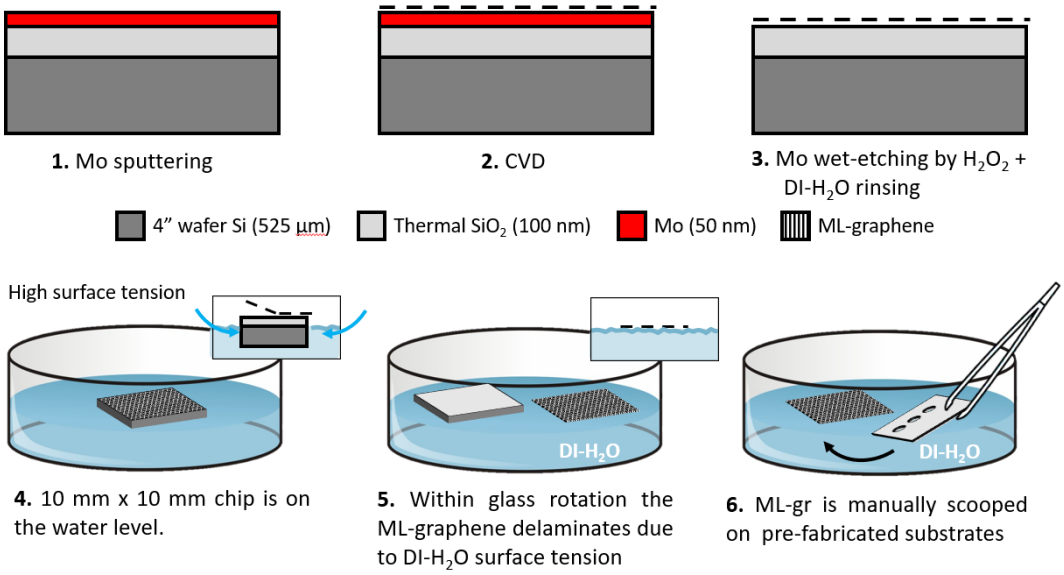

Figure 3.2: The full growth and transfer process of the membranes used in this study.

The silicon chips were etched with Deep Reaction Ion Etching (DRIE) and buffered oxide etch (BOE) to remove the Si_2 hard mask, resulting in holes with a radius of approximately 75, 110 and 250 µm. The chip with suspended graphene membranes was dried for over 10 hours in atmospheric conditions [6]. Imperfections in the form of holes are present with a random distribution and diameter ranging from 20-100 nm in diameter. These imperfections serve as small venting holes, which prevents the bulging of the membrane when any pressure difference is applied.

3.2. Experimental setup

With the membranes provided, we need an experimental setup that can measure and actuate the membranes to investigate the dynamic response. To reduce the effects of squeeze film damping we do the pressure experiments on membranes with a fully etched cavity to isolate the loading effect as much as possible, as can be seen in Figure 3.3 a). Out of the many provided samples, we look for the best membranes based on flatness and tension and wrinkle distribution. We do the visual inspection by using the Keyence VHX-6000 digital microscope with magnification ranging from 20X to 200X. Afterwards, the SPLDV vibrometer is used to look at the velocity response of the surface of the membranes. This is crucial because defects greatly impact the dynamic response. We assume no tension concentration that significantly influences the response for these smooth membranes. An example of such a graphene membrane and a substrate with an array of samples inside the setup is shown in Figure 3.3 b) and c), respectively.

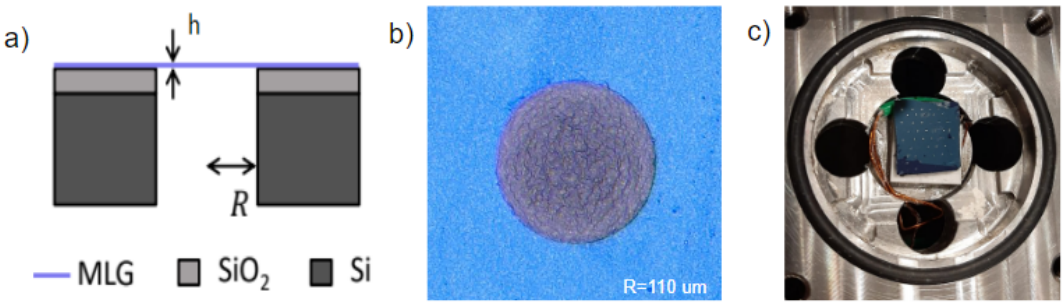

Figure 3.3: a) A schematic representation of the membranes over a cavity used in this study [6]. b) An example of a good membrane (S1). c) A picture of the substrate filled with membranes on top of the piezoelectric shaker.

To study the impact of air loading on graphene membranes, pressure-dependent experiments will be performed to measure the resonance frequency of the membrane's response. The deflection of the membrane will be measured using a single-point laser Doppler vibrometer (SPLDV) setup (OFV-5000 Polytec GmbH). By varying the dimensions of the membrane, the relationship between the radius, thickness, pressure and resonance frequency will be explored. The setup used to characterize the dynamics of the graphene membranes is shown in Figure 3.4.

The Laser Doppler vibrometer is an instrument that uses laser light to measure the velocity of an object's surface vibrations. It works by shining a laser beam onto the surface of an object and measuring the shift in frequency of the reflected light caused by the object's movement. This shift in frequency, known as the Doppler effect, is directly proportional to the velocity of the object's surface. The LDV then converts this frequency shift into the surface velocity [47].

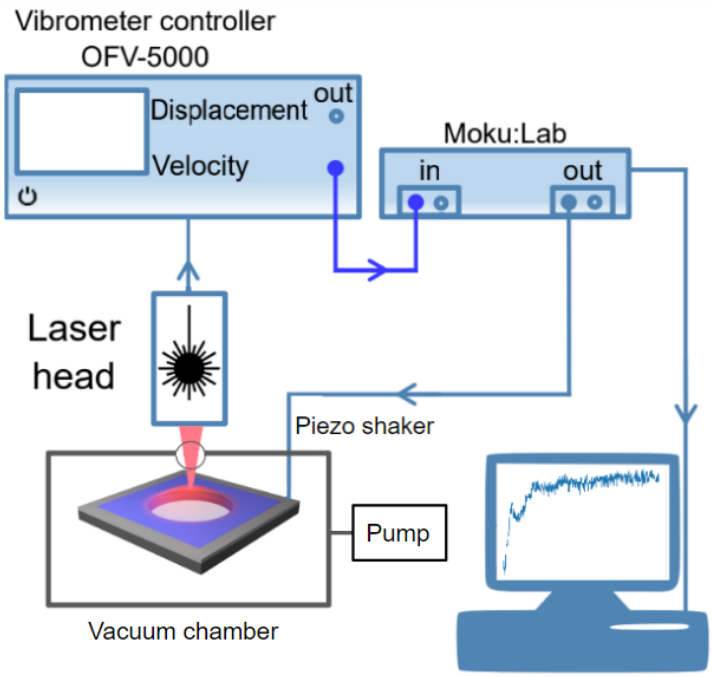

Figure 3.4: Schematic of the single point laser Doppler vibrometer setup. The vibrometer measures the dynamic motion of the graphene membrane as a result of the movement of the piezoelectric shaker underneath the substrate. Measurements are controlled via the Moku:Lab using the spectrum analyzer and frequency response analyser functions. The setup is placed inside a vacuum chamber [6].

The experiment is controlled through a computer via a Moku:Lab FPGA-based signal generator and analyzer, which outputs the driving signal to a piezoelectric actuator and receives a velocity and frequency signal from the SPLDV. The Polytec decoder was predominantly used with a sensitivity of 5 mm/s/V and a measuring range of up to 100 kHz. The piezoelectric actuator was driven at an alternating 400 mV signal.

We initially measured the Brownian motion of many membranes inside the vacuum chamber at atmospheric pressure to understand the various setup parameters and external factors. Since the transfer of graphene causes imperfections like wrinkles and tension concentrations, the maximum displacement for each membrane is not perfectly centred. For consistency and repeatability, the middle of each membrane is measured. It is important to note that while this measurement might not be the exact maximum displacement, it is still a close approximation for better membranes that are used.

The following step was to regulate the pressure with a pump and pressure controller. Since the membranes are very sensitive to any sound or vibrations it was important to closely monitor and reduce the influences of these devices. Since we are working inside a closed vacuum chamber on a passive vibration isolating stage, we assume no other vibrations influencing the response.

For the pressure controller, it was possible to reach pressures in the range of 1 Bar to around 30 mBar. It was not possible to reach lower pressure due to losses in the pressure controller. This range

of pressure was sufficient for the measurements taken.

The results of the pressure sweeps showed similar responses whether the pressure was increasing or decreasing. As more time was needed for relaxation when sweeping downward, the preferred and more efficient method became sweeping the pressure from the lowest to atmospheric pressure. It is worth noting that changes in pressure could lead to the laser being out of focus. This was circumvented by using the relaxation moments between measurement steps to adjust the laser if necessary.

With a reliable way to measure the dynamic response of the middle of the membrane, the next step is to actuate the membrane to increase signal output. Possible options are acoustic actuation, mechanical actuation with for example a piezoelectric element, and electro-thermal actuation. All of these methods show a similar resonance frequency in literature [6]. For microphone application, the most relevant method would be acoustic actuation. However, this is not as viable a method in vacuum environments due to the absents of a medium to propagate the sound. Electro-thermal actuation would require electrical connections to be made on the membrane. Having considered these actuation types, the choice of actuation in this study is mechanical actuation done by a piezoelectric element underneath the substrate. The used piezo-shaker had a good and flat response from 2 kHz to 25 kHz in both air and vacuum as can be seen in measurements in Figure A.6 in the appendix. It should be noted that close to atmospheric pressure, the piezo shaker may act like a speaker as depicted in Figure 3.5. This way the membrane could be actuated via sound and base actuation simultaneously as is further discussed in Chapter 5.

Figure 3.5: Sideview of the setup showing the piezo shaker acting as a speaker as well as base actuation.

It is important to not fully close the cavity underneath the membrane. If it is fully closed, it will lead to squeeze film effects that increase damping and stiffness. Moreover, the limited gas volume inside the closed cavity can not support the significant membrane movement required to produce a large volume change of the (0, 1) resonant mode. As a result, the (1, 1) resonance mode would become dominant, as seen in previous studies on closed cavity resonators [39]. This mode causes minimal volume changes but less displacement in the middle of the membrane.

The two factors preventing this closed cavity effect from happening in this study, thereby having a bigger displacement in the middle of the membrane because of the (0, 1) mode, are firstly the imperfection and perforations inside the membrane to less effectively trap any gasses. Next to that, the substrate is not completely sealed at the bottom and gas can leak away. In the SPLDV setup, rough double-sided tape is used so the substrate is fixed but the air still can enter and escape the cavity.

Even though the SPLDV only measures one single point, it can still be used to get an indication of the mode shape of the membrane. Since the (0, 1) resonant mode should be the biggest in the middle, we can move the laser around and find the largest response. Moving the laser around on the membrane in this way does result in the decrease and increase of peaks on varying frequencies. This is expected behaviour looking at the behaviour of mode shapes on membranes as your looking at different modes.

To more accurately check if what we are looking at is a clear first resonance mode, we use two optical devices. The first setup is a digital holographic microscope (DHM) from Lynceetec paired with a laser-pulsed stroboscopic unit. The second one is a scanning laser Doppler vibrometer setup (SLDV) inside a cleanroom (Iso class 7). Both devices are used to do surface measurements. Figures are shown in Section A.2.

If the air loading is dependent on the density, we can double-check the relation by changing the gas and keeping all other parameters in Equation 2.21 the same. In this study, we used helium to replace the gas inside the chamber.

4

Results

In this section, we will present the most significant findings of the experiments conducted. We investigate the dynamic response of suspended multi-layer graphene over a cavity with changing pressure actuated by a piezoelectric actuator at 400 mV underneath the membrane's substrate. This is done for different geometries with the use of the SPLDV. First, we did the optical inspection with the digital microscope with a magnification of 20X to 200X to look for membranes without big wrinkles or tension concentrations. Around 40 membranes of $D = 110$ µm and 20 with $D = 250$ µm were used in different qualities. In the end, out of the around thousand measurements consisting of approximately 40 full pressure sweeps, most measurements were done on five membranes of $D = 110$ µm and 10 of $D = 250$ µm. The measurements on the smaller membranes were done earlier in the process. The selected membranes are placed inside the vacuum chamber and investigated by the SPLDV. The membranes that are used for the figures in Section 4 and the appendix are mentioned in Table 4.1. Here B1, B2 and B4 are the only ones from the same substrate.

The SPLDV uses 512 sweep points that are linearly distributed between 2-100 kHz. Furthermore, the settling time is 15 µm, the averaging time is 30 ms and one cycle and settling cycle are used. With these settings, a single measurement took around ten seconds. Together with the relaxation time of around 20 seconds, a full sweep through 20 different pressures took around ten minutes. Additional measurements were done as well as measurements for reference on the substrate and the piezo shaker, which can be found in Appendix A.2. The value for the NAVMI for the first mode $\Gamma = \frac{2}{3}$ is used [30, 34].

110 µm membranes

The response of the membrane S1 with the size of $R = 110$ µm is shown in a waterfall plot in Figure 4.2. It should be noted that the first peak decreases and other peaks emerge when moving the laser from the centre. This happens to the point that we reach the silicon substrate.

A different visualization of the data is done in the colour plot in Figure 4.2. Here the air loading model from Equation 2.21 and fit parameters $n_0 = 0.7$ N/mm and $t = 4$ nm is added.

Table 4.1: The membranes used for the figures in this report.

Sample	Radius [um]	Thickness [nm]	Tension [N/mm]
S1	110	4	2.5
B1	250	9	7.5
B2	250	9	7.5
B3	250	13	2.5
B4	250	9	2.05

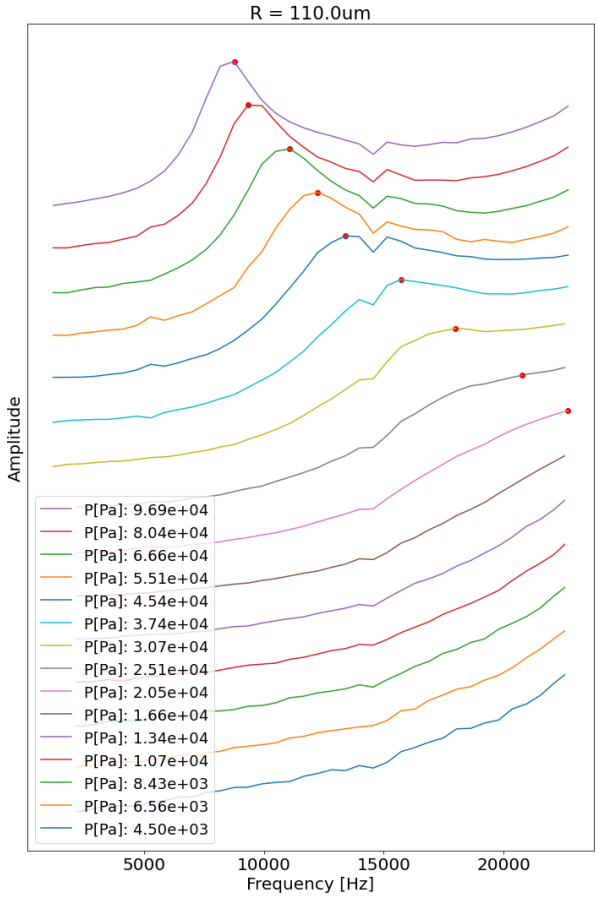

Figure 4.1: The dynamic response of the graphene membrane S1 (R=110 µm) with changing pressure measured with the SPLDV in air. The red dots indicate the course of the first peak.

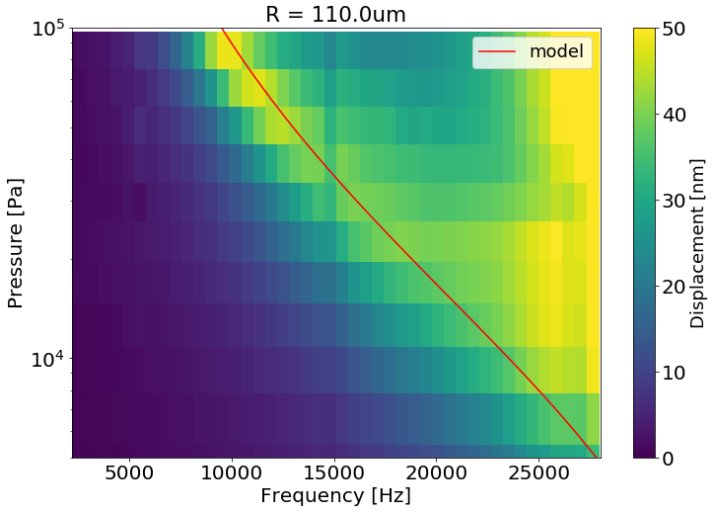

Figure 4.2: A colour plot of the dynamic response of the graphene membrane S1 ($R = 110$ µm) with changing pressure measured with the SPLDV in air. Added with the model according to Equation 2.21 and fit parameters $n_0 = 0.7$ N/mm and $t = 4$ nm.

250 µm membranes

We do similar measurements on larger graphene membranes to verify if bigger membranes also show a bigger influence on the air loading. A waterfall plot of sample B1 can be seen in Figure 4.3 and a colour plot with the model of the resonance frequency according to Equation 2.21 is plotted in Figure 4.4.

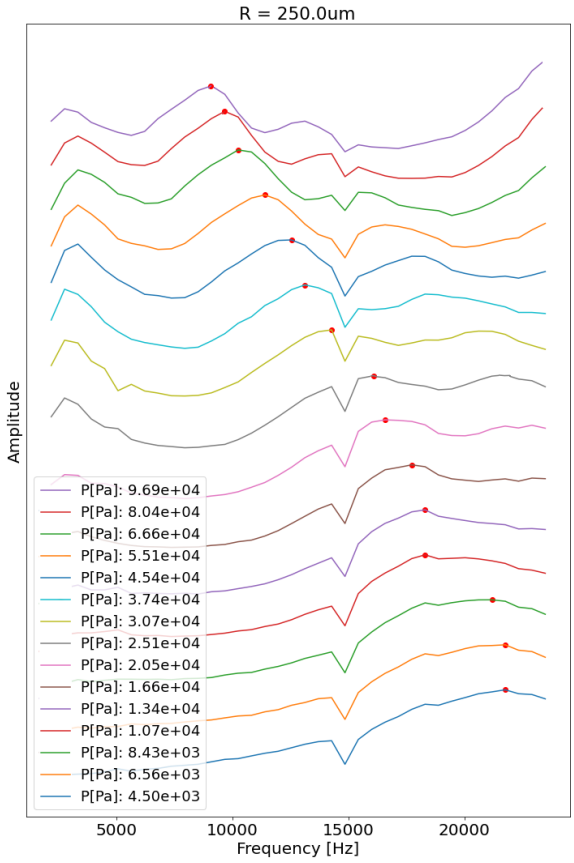

Figure 4.3: The dynamic response of the graphene membrane B1 (R= 250 µm) with changing pressure measured with the SPLDV in air. The red dots indicate the course of the first peak.

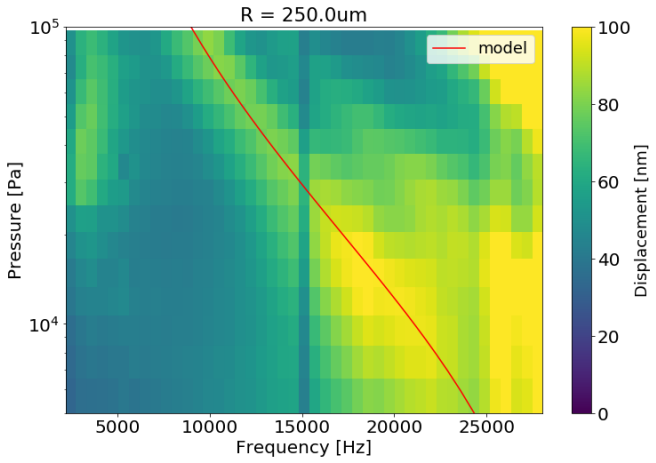

Figure 4.4: A colour plot of the dynamic response of the graphene membrane B1 (R = 250 µm) with changing pressure measured with the SPLDV in air. Added with the model according to Equation 2.21 and fit parameters n_0 = 7.5 N/mm and t = 9 nm.

Helium measurements

To verify the gas dependency of the mass loading phenomena, we did measurements in a different gas too. With all membrane parameters the same, we expect the formula to be as in Equation 4.1. Results of such measurements with the helium model incorporated can be seen in Figure 4.5.

$$f_0(P) = \frac{2.405}{2\pi R}\sqrt{\frac{n_0}{\rho_g h_g + \Gamma\rho_{He}(P)R}}. \tag{4.1}$$

The same membrane is used in figures 4.3 and 4.5.

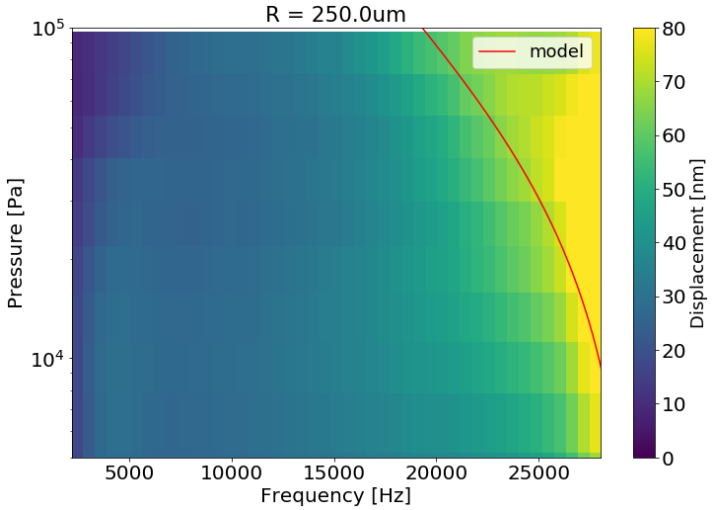

Figure 4.5: Dynamic response of graphene membrane B1 (R = 250 µm) with changing pressure measured with the LDV in Helium. a) Color plot of graphene membrane. Added with the model according to Equation 2.21 and fit parameters n_0 = 7.5 N/mm and t = 9 nm. b) Waterfall plot with the first peak marked for extra clarification.

5 Discussion

This section aims to interpret the results and explain their significance. We will provide an explanation of the implications of the results. Additionally, we will consider the broader context of the findings and their relevance in the field of MEMS microphones.

5.1. Discussion on experimental setup and findings

The results of the study for both sizes of membranes in Section 4 demonstrate that the conducted experiments have produced similar outcomes to be expected from the models of the resonance frequency with the air loading effect. By slightly varying thickness and different radii in the measurements as can also be seen in Section A.2, we can conclude that the model of Equation 2.21 based on the acoustic radiation impedance is a good approximation of the effect that we are seeing in this study. This study contributes as evidence for the validity of this model, which can be used for future research in the field of acoustic sensors with nanometer-thin sensing membranes in or close to ambient pressures.

The setup was designed and used to isolate the air loading effect as much as possible from other effects. However, some scenarios or assumptions still deserve further attention. Starting with the imperfections caused by the fabrication method. Because of the high influence of wrinkles and folds on the dynamic response, many membranes have been optically and dynamically inspected to select the best membranes with an even tension distribution as seen in Figure 3.3 b). Examples of bad samples can be found in Figure 5.1. These membranes have visible wrinkles in them and show unpredictable mode shapes and resonance behaviour similar to that in literature [10].

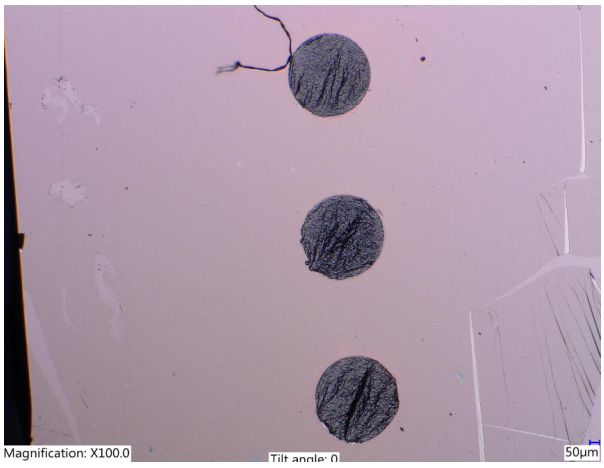

Figure 5.1: Three examples of unused graphene membranes looked at through the Keyence digital microscope.

The dynamic inspection was done by scanning the surface of the membrane with the SPLDV. A flat membrane would show no heavy scattering of the laser due to the absence of uniformities. Another

characteristic that flat membranes showed was a symmetric frequency response when moving the laser away from the centre in all directions. The visible first frequency peak, similar to those in 4.1, would decrease when moving around and other peaks showed up. These peaks indicate other modes of the membrane.

When fitting the model on the data, it should be noted that the tension and thicknesses were not measured for every sample. Since the fabrication process creates the mentioned imperfections like varying thicknesses and tension, an approximation is made based on measurements done on similar samples. The membranes on the same wafer did have an identical growth rate to reduce process variations, resulting in a thickness variation of around 25%.

A drawback when studying the ultrathin but large-diameter graphene membranes was the collapsing of the membranes after a few months. The membranes having extra tension concentration were more susceptible to breaking by shocks induced by the placement and carrying of the substrate, which is expected due to the worse quality. For measurements taken on high-quality membranes, this deterioration could not be detected in the dynamic response.

One of the major limitations of the SPLDV setup was the limited bandwidth of the piezo-shaker. Starting the measurements without piezo actuation, the air loading effect was already visible because of the Brownian motion. However, for Brownian motion, external influences like vibrations from the pressure controller could be detected too sometimes as is shown and discussed in the appendix Figure A.5. This caused us to use the piezoelectric element to increase the response. Having a limited flat response up to 25 kHz caused no problems for most membranes. Only for membranes with higher resonances, including the helium measurements, did the limited bandwidth cause the higher frequency measurements to become unusable. With the validation of the Brownian motion showing similar air loading effects when measuring the membranes for higher frequency membranes, we were confident that the membranes that showed resonances below 25 kHz were sufficient to study the air loading effect on the membranes in and close to the setup limit.

Throughout the measurements, we assumed the pumping is not done adiabatically because of the high relaxation time and the chamber being an open system. We can therefore view the measurements to be done at the same temperature. This assumption is important because of the effect that temperature has on the dynamics through induced stresses.

Another interesting scenario to consider is one of the membranes being actuated by the piezo through the medium together with the base actuation as seen in Figure 3.5. Since the membranes are highly sensitive to changes in pressure, the piezo-shaker could act as a speaker which would actuate the membrane when the pressure is close to atmospheric. This would combine to the following simplified equation of motion of a membrane with air loading:

$$[M_{\text{membrane}} + \beta M_{\text{air}}]\,\ddot{q} + C\dot{q} + Kq = F_{\text{base}}(\omega) + F_{\text{air}}(\omega). \tag{5.1}$$

Furthermore, we assumed the cavity, with depth $g = 520$ µm which is equal to the thickness of the substrate, to not be fully sealed. Leakage is possible through the membrane itself as well as at the bottom of the substrate. If this was not the case as demonstrated in Figure 5.2, we would not see a mode (0, 1) because of the large change in the volume necessary similar to that in [39]. A closed cavity would also result in an extra pressure-dependent stiffness. For a closed cavity the pressure P or volume V should stay the same when the membrane is moving. This results in the relation $P_0V_0 = P_1V_1 =$ Constant. For a small displacement Δx there will be a small change in volume resulting in a force

$$\Delta F = \frac{-P_0V_0}{g^2}\Delta x. \tag{5.2}$$

This gives the following stiffness

$$K_{\text{air}} = \frac{P\pi R^2}{g}. \tag{5.3}$$

This stiffness would be parallel to the low stiffness of the membrane. For a closed cavity without air loading in ambient pressure, this would result in a very high resonance frequency that would decrease with pressure as can be seen in Figure 5.3. In lower pressures, where there is less air, the stiffness is significantly lower which decreases the resonance frequency. This is not observed in this study, in fact we see the resonance frequency decrease with higher pressures. From this observation, we conclude

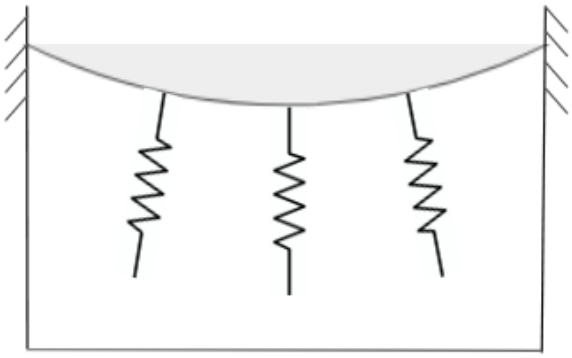

Figure 5.2: A schematic of a closed cavity resonator with springs indicating the extra stiffness present due to the compression of air. This stiffness is parallel to that of the membrane. The cavity depth $g = 520$ µm is equal to the thickness of the substrate.

that either the back volume is open enough and/or the membrane is sufficiently permeable, such that so-called squeeze-film effects, shown in Fig. 5.2, have little effect on the resonance frequency.

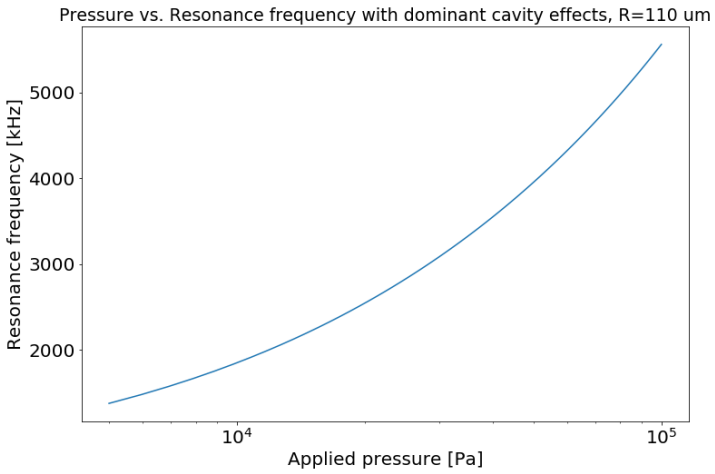

Figure 5.3: Example of a typical membrane (R=110 µm, N_g= 7.2e-3 N/m) with a dominant air stiffness as a result of closed cavity effects.

Based on the observation of the (0, 1) mode and significantly lower resonance frequencies (by a factor of 1000) when measuring at lower pressures compared to the model with added air stiffness, it appears that the air loading effect is well isolated from the added stiffness caused by cavity effects.

Finally, the helium experiments had an expected higher resonance frequency as can be seen in Figure 4.5. It was however difficult to measure the full range of pressures when using the helium. The higher resonance reached out of range for the measurement setup. However, for the measurements that were in range, we could see a similar course to that of the model. It is a good sign that on the same membrane with the same fitting parameters, we see a good fit for the loading effect model on both air and helium. This validates the dependency on the medium of mass loading.

5.2. Theoretical limits of microphone sensitivity with limited bandwidth

It is of high importance that the bandwidth of a microphone is at a minimum as high as the operating range. This bandwidth is limited by the resonance frequency according to the linear oscillator model. For the membranes measured in this research, the extremely large diameter compared to thickness results in very high mechanical sensitivities according to Equation 1.5. However, because of the air

loading effect, the bandwidth is very limited. The possible increase in mechanical sensitivity by using large aspect ratio membranes is not achievable without a loss in bandwidth. If a microphone with a bandwidth and resonance frequency outside the audible range is required, this should require an increase in tension. This increase does lower the mechanical sensitivity. The required tension needed to reach a certain resonance frequency in a vacuum can be calculated with the formula for the resonance frequency

$$\omega_{mn} = \frac{\alpha_{mn}}{R}\sqrt{\frac{n_0}{\rho h}}. \tag{5.4}$$

Rewriting this and combining it with Equation 2.19, we obtain the tension required to reach a specific bandwidth ω_{BW}.

$$n_{0,BW} = (1+\beta)(\omega_{BW}^2 R^2 \rho_g h_g)/2.405^2. \tag{5.5}$$

A plot of this relationship is shown in Figure 5.4. It becomes clear that for thinner membranes when the air loading becomes dominant, a far higher tension is required to reach the same bandwidth. This effect is negligible for thicker membranes ($h_g > 300$ nm).

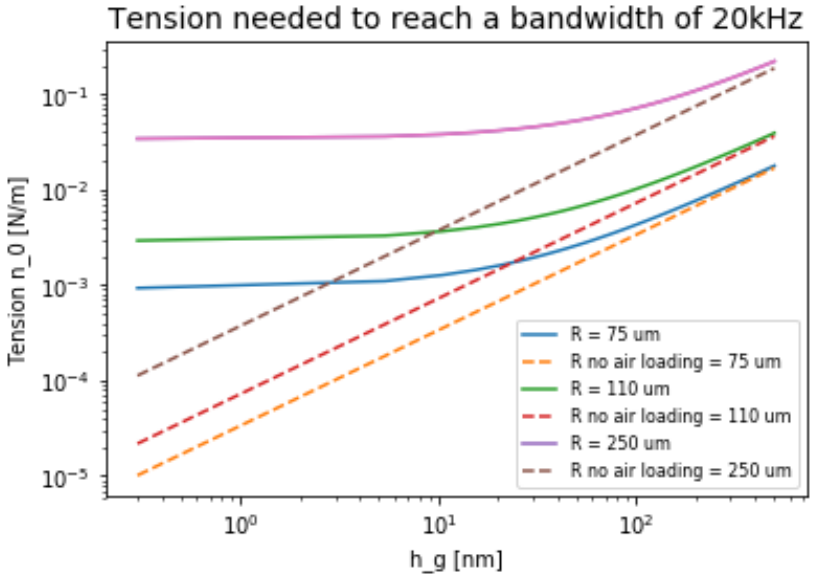

Figure 5.4: The tension needed for a membrane of a specific thickness and radius to reach a bandwidth or resonance frequency of 20 kHz according to Equation 5.5. This is plotted for both cases where air loading is and is not accounted for.

Table 5.1: Tensions and estimated tension of membranes used in this report.

Sample	Measured resonance in air [kHz]	Tension required according to Equation 5.5 [N/mm]
S1	10	1
B1	9	10
B2	9	10
B3	5	2.5
B4	5	2.5

Above in Table 5.1 a summation of the values measured for the different resonance frequencies is done together with the expected tension as derived from Equation 5.5. Differences in the resonance frequency to other microphone studies can be explained by having different morphology which as mentioned before heavily influences the dynamic response. Next to that, there could be a different dynamic response between the actuation type used in this study and sound actuation.

When first looking at Equation 1.5, it becomes clear that making the sensing membrane bigger and thinner would increase the sensitivity without limitations. After doing experiments in the extremes of

possible dimensions with the help of graphene, it became clear that the effect of air loading plays a major role on the resonance frequency similar to those of mass loading in other fluids as mentioned in other studies [23, 25, 48]. The high resonance which is expected for low mass membranes, looking at Equation 2.2, is not realistic anymore because of the air loading. The trade-off between mechanical sensitivity and resonance frequency becomes clear when using Equation 1.5 and the tension needed for a specific resonance as derived in Equation 5.5 to derive the following equation for the mechanical sensitivity:

$$S_m = \frac{2.405^2}{8\omega_{BW}^2 \rho_g h_g (1 + \Gamma \frac{\rho_{air}}{\rho_g} \frac{R}{h_g})}. \tag{5.6}$$

When plotting this equation for multiple radii as in Figure 5.5, we can conclude that decreasing the thickness does increase the mechanical sensitivity. However, for a set bandwidth (20 kHz in this case) we get a lower possible sensitivity when keeping the air loading effect into account. Without air loading, we would get a relation that is not dependent on the radius. This explains why for thicker membranes when the air loading is not dominant, the radius does not affect the mechanical sensitivity as much. However, for membranes of single (0.3 nm) or multi-layer graphene, we see a considerable decrease in the possible sensitivity that is dependent on the radius of the membrane. For smaller radii of membranes, we reach the maximum sensitivity at smaller thicknesses. This relation suggests that the largest sensitivities are reached for small and thin membranes when there is a set bandwidth. This is considered when all tensions are possible to be fabricated.

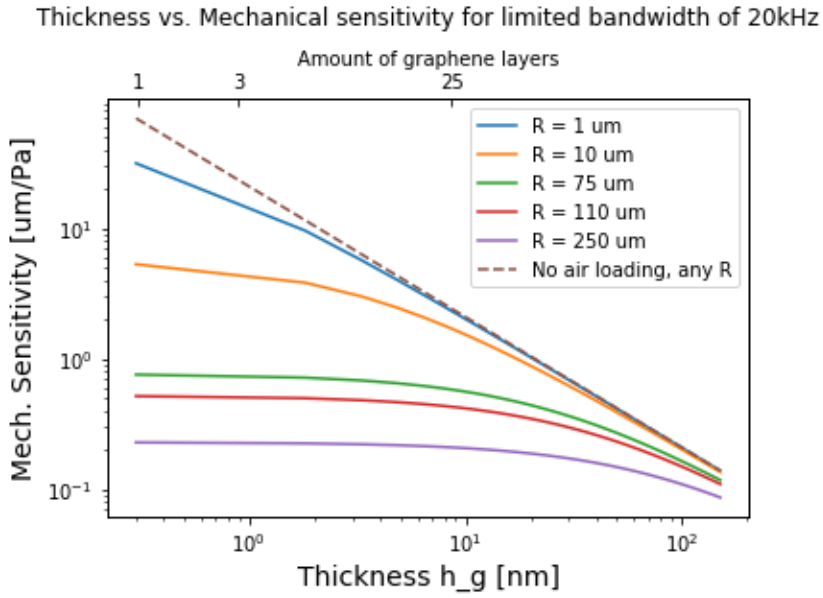

Figure 5.5: Theoretic maximum of the mechanical sensitivity as described by Equation 5.6 for different sizes of membranes when the bandwidth is limited to 20 kHz. The dashed line is when no air loading is accounted for. The amount of graphene layers roughly corresponding to the thickness is added.

5.3. Road to commercial microphones

With many new challenges to overcome to increase performance in graphene MEMS microphones, breakthrough research in transfer-free fabrication make it more realistic than ever to realize a high-performance graphene microphone for mass production [20]. With the possibility for larger and higher quality graphene membranes, an increase in performance was proven. However, the air loading effect is limiting the bandwidth of these devices. Next to the fabrication and performance trade-off that has to be made when designing graphene membranes, an essential part of these sensors is the readout method. Options would be optical or condenser readout. Both of them have different difficulties to overcome to be used effectively. For optical readout, as used in this research, we would need novel

packaging techniques to do the readout in a size-effective way. For condenser readout, there are many difficulties around the air gap. For this readout type, you want the air gap as small as possible to have a large electrical sensitivity as can be seen in Equation 1.4. A small air gap does decrease the pull-in voltage of the microphone as explained in A.3. Next to that it also causes a bigger contribution of the squeeze film effects as explained in A.1. To conclude, while graphene MEMS microphones have a lot of potential, several challenges must be addressed to be ready for commercial use. The air loading effect is one such challenge that heavily impacts the microphone's bandwidth, but there are also additional hurdles such as fabrication difficulties and selecting the most effective readout method that must be carefully researched and overcome to bring graphene MEMS microphones to market.

6

Conclusion and recommendations

In conclusion, this thesis has demonstrated the significant influence of the air loading effect on the resonance frequency of nanometer-thin graphene membranes, showing high resonance frequencies and bandwidths in a vacuum but low resonance frequencies in ambient pressure. Through the use of pressure-dependent experiments, this thesis has provided evidence supporting the applicability of the theory of acoustic radiation impedance on nanometer-thin graphene membranes. This theory can be used to map the limitations of acoustic sensitivity with limited bandwidth. These findings highlight the importance of considering the effect of air loading when designing MEMS microphones and provide valuable insights into the trade-off between mechanical sensitivity and bandwidth. To design the optimal microphone, it is necessary to minimize the air loading effect, which can be achieved by using a smaller sensing membrane or even better, an array of these membranes. By using more membranes in an array, the signal can be increased. For higher sensitivity, membranes with smaller radii are preferred. These membranes can reach the same bandwidth with lower tension. Although this lower tension increases the mechanical sensitivity, it is still challenging to achieve as low tension with current fabrication techniques.

Multi-layer graphene membranes show the potential to be used for highly sensitive microphones. However, the air loading effect can not be ignored, specifically for larger-size membranes of nanometer thickness. The use of many arrays of smaller sensing membranes should be researched to reach high sensitivity and bandwidth. Also, further research could be conducted on the use of other gases for a mass loading gas sensor design. Furthermore, it would be interesting to research the effects of the air loading on the damping and noise of these membranes. For the focus of microphones with capacitive readout microphones, the effects of an added backplate should be explored in greater depth and investigated if this readout method is still feasible for these dimensions of microphones. Overall, this thesis has contributed to the understanding of the air loading effect on thin graphene membranes which can support the development of high-performance graphene-based MEMS microphones.

Acknowledgements

I would like to acknowledge all support from European Union's Horizon 2020 research and innovation program under Grant Agreement No, 881603 (Graphene Flagship). Furthermore, I would like to thank Peter, Gabriele and Roberto for their guidance during this research.

I would like to thank friends and family for supporting me through the many wonderful years I had at this university. Additional thanks to the study association Taylor and everyone involved in this great Master's program.

A

Appendix

A.1. Squeeze film damping

The squeeze film effect occurs when a thin film is compressed between two surfaces visible in Figure A.1.

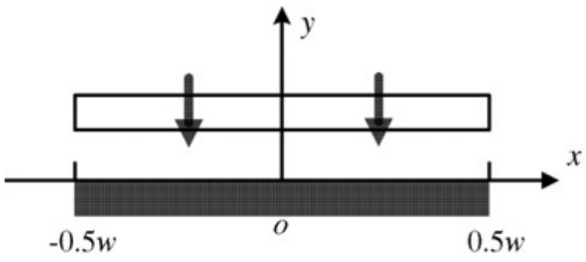

Figure A.1: Squeeze film air damping cross-sectional view [22].

The squeeze film effect occurs in two regimes shown in Figure A.2. In the first regime which is applicable for lower frequencies, the damping force is dominant. The second regime applies to higher frequencies of the membrane in which the elastic force is dominant (assuming no changes in the other parameters). These regimes are described by the squeeze number σ [22]:

$$\sigma = \frac{12\mu\omega_s l^2}{P_a g_0^2}. \tag{A.1}$$

Where μ, ω_s, P_a and g_0 are the viscosity of the fluid, radial frequency, ambient pressure and initial air gap or film thickness, respectively.

When a graphene membrane is moving at low frequencies, the gas can enter and escape the gap region of a capacitive microphone (see Figure 1.1) so that the pressure stays constant [5]. The mechanical damping is reduced when increasing the air gap or the number and size of perforated holes. These losses in the cavity, R_{cavity} is described by Skvor's formula [49]:

$$R_{cavity} = \frac{12\mu_{air}}{\pi n_h g_0^3} B(A_r). \tag{A.2}$$

where μ_{air} is the viscosity of air and n_h is the number of backplate holes. The term A_r is the ratio of the total area of the backplate holes to the area of the backplate, and $B(A_r)$ is defined as:

$$B(A_r) = \frac{1}{4} ln(\frac{1}{A_r}) - \frac{3}{8} + \frac{1}{2}A_r - \frac{1}{8}A_r^2. \tag{A.3}$$

However, at high resonance frequencies, the air is trapped because of the viscous forces. If the resonance frequency is much higher than the time it takes to escape the cavity, the gas applies an

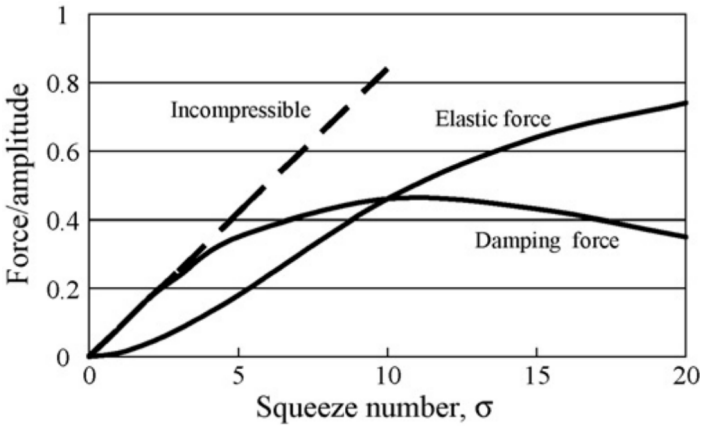

Figure A.2: The dependence of viscous damping force and elastic force on squeeze number [22].

elastic force to the system which adds stiffness. This results in an increase of the resonance frequency ω by [5, 50]:

$$\omega^2 = \omega_0^2 + \frac{P_a}{g_0 \rho h}. \tag{A.4}$$

Where ω_0 is the mechanical resonance frequency in a vacuum and ρh is the membrane's mass per square metre. For the lower resonances at which microphones operate the squeeze number is low, therefore the squeeze film effect dampens the sensing membrane. However, the holes in multilayer graphene membranes are due to imperfections in the membrane. Therefore a circular plate might be a better approximation of the system. For a circular plate, the coefficient of damping is given as [22]:

$$c_{cir} = \frac{3\pi}{2g_0^3}\mu R^4. \tag{A.5}$$

A.2. Extra measurements

For the validation of the air loading effect the most significant measurements are the ones done on the membranes themselves. Some more measurements on membranes are shown in figures A.3 and A.4.

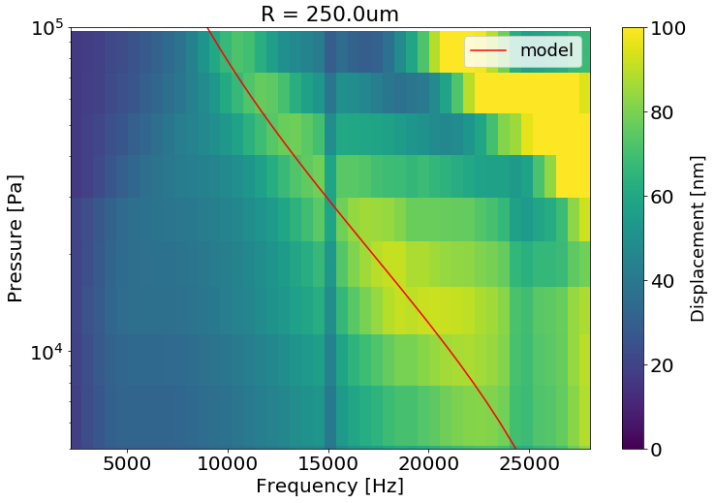

Figure A.3: A colour plot of the dynamic response of the graphene membrane B2 (R=250 µm) with changing pressure measured with the SPLDV in air. Added with the model according to Equation 2.21 and fit parameters n_0 = 7.5 N/mm and t = 9 nm.

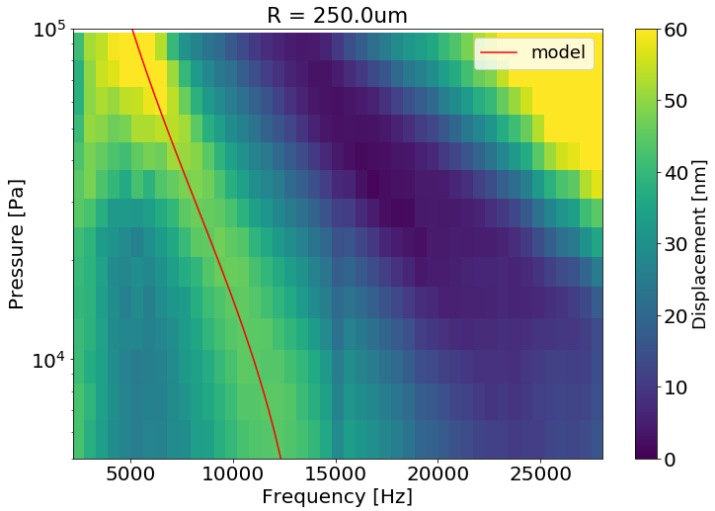

Figure A.4: A colour plot of the dynamic response of the graphene membrane B3 (R=250 µm) with changing pressure measured with the SPLDV in air. Added with the model according to Equation 2.21 and fit parameters $n_0 = 2.5$ N/mm and $t = 13$ nm.

At the start of this research, we looked at Brownian motion to understand all external factors that could influence the response of the dynamic response. The limitations of the setup became more clear. When no actuation was performed on the membrane, it could pick up a ringing noise at a frequency of 6 kHz coming from the pressure controller as can be seen in Figure A.5. This ringing was very soft but could be heard and decreased at lower pressures as expected of sound. Similar to the ringing sound the membrane was able to pick up sounds when played by a speaker, proving the sensitivity of the membrane to sounds and external actuation. The tension used to fit the model is higher for the actuated motion. This can be explained by extra tension that is induced when the membranes are actuated.

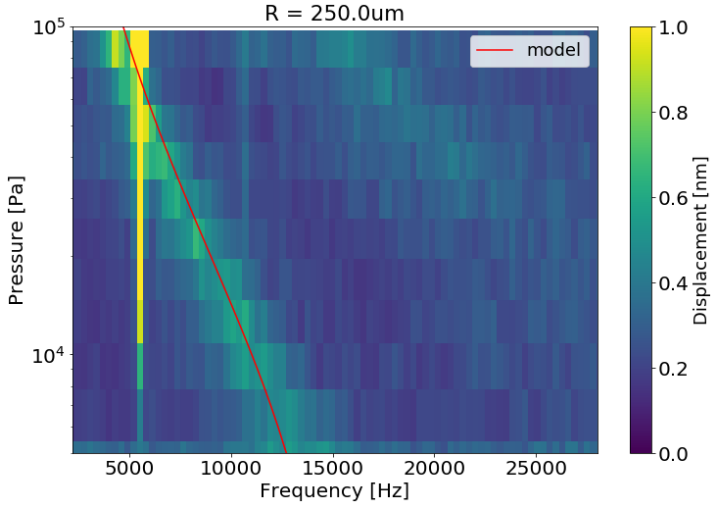

Figure A.5: A colour plot of the Brownian motion (no actuation) of the graphene membrane B4 (R=250 µm) with changing pressure measured with the SPLDV in air. Added with the model according to Equation 2.21 and fit parameters $n_0 = 2.05$ N/mm and $t = 9$ nm.

The same measurements were also done on the piezoelectric actuator used in this study as seen in Figure A.6 as check. The measurement done on the substrate can be seen in Figure A.7.

It is important that both the piezo and substrate move the same amount. This way the substrate is properly fixed to the membrane. For most frequencies, this seems to be the case for the measured

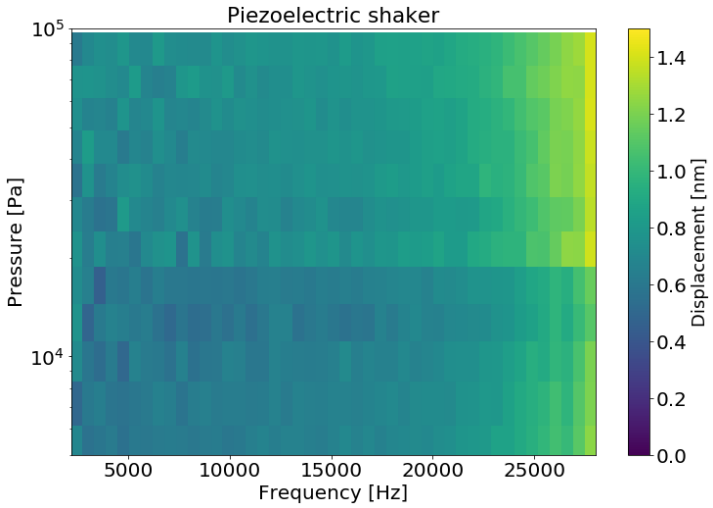

Figure A.6: A colour plot of the measurement taken of the piezoelectric actuator directly used to confirm the limited bandwidth.

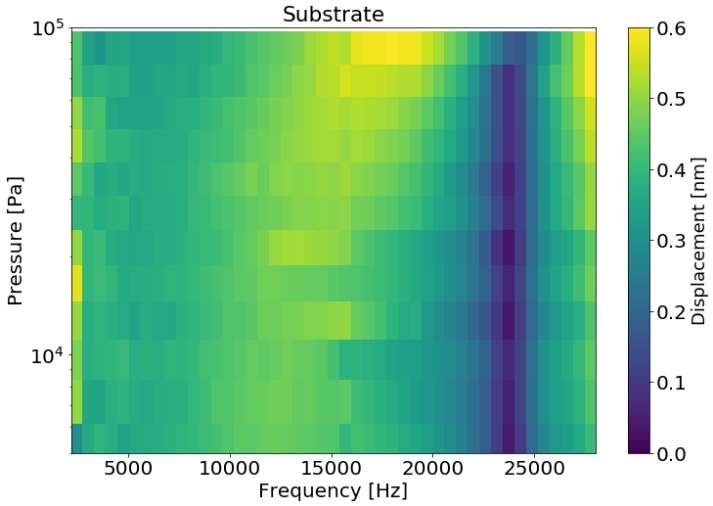

Figure A.7: A colour plot of a measurement taken of the silicon dioxide substrate with graphene transferred over it.

substrate. Between different substrates there will be differences due to the placement, weight, shape or tape.

To check if we are actually looking at the (0, 1) mode we use the Lynceetec digital holographic microscope. We find a nice first mode as seen in Figure A.9.

A similar check on the modes was done on the scanning laser Doppler vibrometer. Again we see a nice representation of what would be a (0, 1) mode.

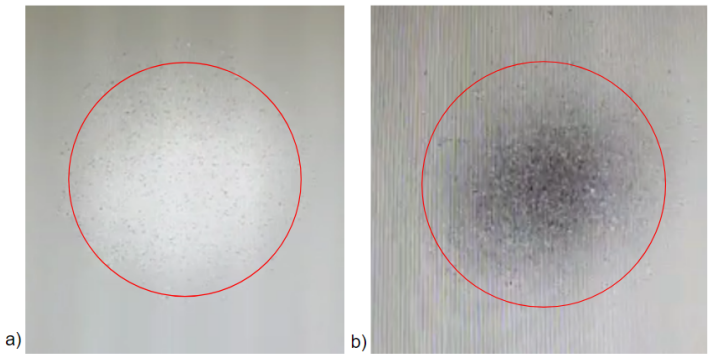

Figure A.8: A snapshot of the first mode of a membrane B2 (R=250 µm) in the Lynceetec at atmospheric pressure. There was no use of tape in this experiment a) Maximum position, b) minimum position of the displacement.

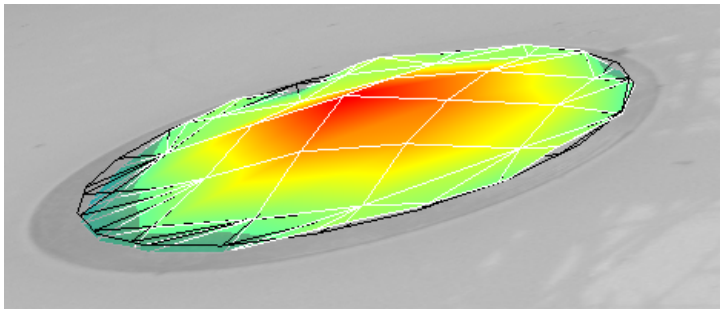

Figure A.9: A snapshot of the first mode of a membrane B3 (R=250 µm) in the SLDV at 9 kHz at 0.3 mbar.

Parylene measurements

Since the effect of air loading is heavily dependent on the thickness of the membrane, we have tried to increase the thickness by adding a layer of parylene to the graphene. However, the membranes were not of good quality having all sorts of wrinkles and stress concentrations as can be seen in Figure A.10. When trying to measure them underneath the LDV setup, the measurements were unusable. This once again shows the importance of good-quality membranes when working on the nanometer scale.

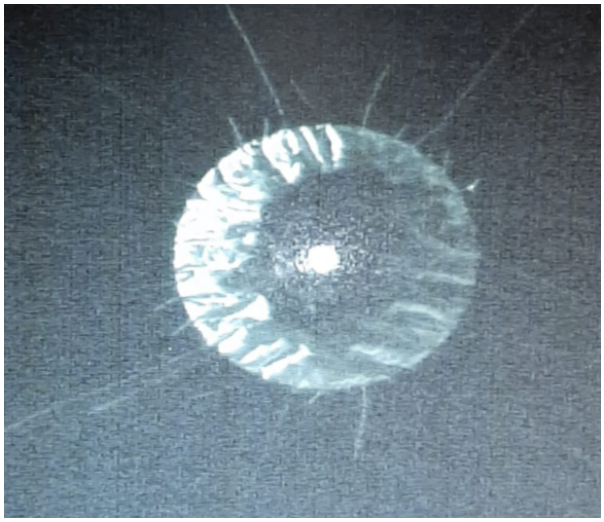

Figure A.10: An example of a multi-layer membrane ($R = 110$ µm) made of parylene and graphene looked at through the SPLDV setup. The laser tip is pointing in the middle of the membrane.

A.3. Failure modes

Due to large mechanical sensitivity and displacements in graphene membranes, extra awareness should be for failure modes. For graphene microphones with low tension, specifically, the pull-in voltage and stiction failure should be accounted for in the device's design. Next to that, the failure modes for general capacitive MEMS microphones, dust/particle damage and water entry are depicted in Figure A.11 [51].

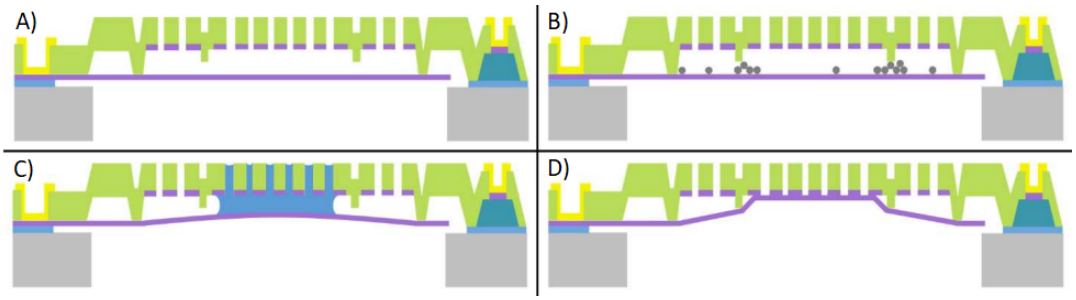

Figure A.11: Capacitive MEMS microphones in various failure modes: A) Normal, B) dust/particle damage, C) water entry, D) stiction failure [51].

It is impossible to keep high performances without being prone to any of these failure modes. For example particle damage, it would be best to have no interference between the membrane and its surroundings to let the maximum signal through to the diaphragm. No shielding would however cause these particles to enter and stack up, eventually obstructing the motion as can be seen in Figure A.11 B). For applications like mobile devices and hearing aid, the devices are designed to be splash-proof. Water and humidity can cause serious damage to the device by causing stiction issues visible in Figure A.11 C). Stiction can also be due to other factors like a mechanical shock, acoustic overload or the pull-in voltage. Sudden accelerations or high amplitude waves can cause the diaphragm to move towards the backplate. When in contact they clamp together due to electrostatic forces, damaging the device visible in Figure A.11 D).

The stiction failure mode can also come due to the electrostatic forces becoming greater than the mechanical force. At the pull-in voltage, V_p the membrane collapses with the fixed ground plate. The pull-in voltage can be calculated by using the effective spring stiffness of the membrane k, the gap at zero voltage d_0, the permittivity of air ϵ and the area of the membrane A_e by the following equation [52]:

$$V_p = \sqrt{\frac{8}{27}\frac{kd_0^3}{\epsilon A_e}}. \tag{A.6}$$

With the effective spring stiffness calculated with:

$$k = 8\pi\sigma_d h. \tag{A.7}$$

Where σ_d is the tensile stress of the membrane.

Bibliography

[1] Changgu Lee et al. “Measurement of the elastic properties and intrinsic strength of monolayer graphene”. In: *science* 321.5887 (2008), pp. 385–388.

[2] A. K. Geim. “Graphene: Status and Prospects”. In: *Science* 324.5934 (June 2009). Publisher: American Association for the Advancement of Science, pp. 1530–1534. DOI: 10.1126/science.1158877. URL: https://www.science.org/doi/full/10.1126/science.1158877 (visited on 02/11/2022).

[3] J. Scott Bunch et al. “Impermeable Atomic Membranes from Graphene Sheets”. en. In: *Nano Letters* 8.8 (Aug. 2008), pp. 2458–2462. ISSN: 1530-6984, 1530-6992. DOI: 10.1021/nl801457b. URL: https://pubs.acs.org/doi/10.1021/nl801457b (visited on 11/04/2021).

[4] Andrea C. Ferrari et al. “Science and technology roadmap for graphene, related two-dimensional crystals, and hybrid systems”. en. In: *Nanoscale* 7.11 (2015), pp. 4598–4810. ISSN: 2040-3364, 2040-3372. DOI: 10.1039/C4NR01600A. URL: http://xlink.rsc.org/?DOI=C4NR01600A (visited on 12/17/2021).

[5] Peter G Steeneken et al. “Dynamics of 2D material membranes”. en. In: *2D Materials* 8.4 (Oct. 2021), p. 042001. ISSN: 2053-1583. DOI: 10.1088/2053-1583/ac152c. URL: https://iopscience.iop.org/article/10.1088/2053-1583/ac152c (visited on 10/20/2021).

[6] Gabriele Baglioni et al. “Ultra-sensitive graphene membranes for microphone applications”. In: *arXiv preprint arXiv:2211.03369* (2022).

[7] Dejan Todorović et al. “Multilayer graphene condenser microphone”. en. In: 2.4 (Nov. 2015). Publisher: IOP Publishing, p. 045013. ISSN: 2053-1583. DOI: 10.1088/2053-1583/2/4/045013. URL: https://doi.org/10.1088/2053-1583/2/4/045013 (visited on 10/20/2021).

[8] H. Cheun Lee et al. “Review of the synthesis, transfer, characterization and growth mechanisms of single and multilayer graphene”. en. In: *RSC Advances* 7.26 (2017), pp. 15644–15693. ISSN: 2046-2069. DOI: 10.1039/C7RA00392G. URL: http://xlink.rsc.org/?DOI=C7RA00392G (visited on 03/09/2022).

[9] Florian Banhart, Jani Kotakoski, and Arkady V. Krasheninnikov. “Structural Defects in Graphene”. en. In: *ACS Nano* 5.1 (Jan. 2011), pp. 26–41. ISSN: 1936-0851, 1936-086X. DOI: 10.1021/nn102598m. URL: https://pubs.acs.org/doi/10.1021/nn102598m (visited on 03/09/2022).

[10] C Wang et al. “Abnormal frequency characteristics of wrinkled graphene”. In: *RSC Advances* 4.18 (2014), pp. 9395–9400.

[11] Yelena Grachova et al. “High quality wafer-scale CVD graphene on molybdenum thin film for sensing application”. In: *Procedia Engineering* 87 (2014), pp. 1501–1504.

[12] Jacob Fraden. “Microphones”. en. In: *Handbook of Modern Sensors: Physics, Designs, and Applications*. Ed. by Jacob Fraden. Cham: Springer International Publishing, 2016, pp. 485–505. ISBN: 978-3-319-19303-8. DOI: 10.1007/978-3-319-19303-8_13. URL: https://doi.org/10.1007/978-3-319-19303-8_13 (visited on 12/02/2021).

[13] Siti Aisyah Zawawi et al. “A Review of MEMS Capacitive Microphones”. en. In: *Micromachines* 11.5 (May 2020). Number: 5 Publisher: Multidisciplinary Digital Publishing Institute, p. 484. DOI: 10.3390/mi11050484. URL: https://www.mdpi.com/2072-666X/11/5/484 (visited on 10/20/2021).

[14] Marc Fueldner. “Microphones”. en. In: *Handbook of Silicon Based MEMS Materials and Technologies (Third Edition)*. Ed. by Markku Tilli et al. Micro and Nano Technologies. Elsevier, Jan. 2020, pp. 937–948. ISBN: 978-0-12-817786-0. DOI: 10.1016/B978-0-12-817786-0.00048-7. URL: https://www.sciencedirect.com/science/article/pii/B9780128177860000487 (visited on 04/28/2022).

[15] *Damping in Structural Dynamics: Theory and Sources*. fr. URL: https://www.comsol.fr/blogs/damping-in-structural-dynamics-theory-and-sources/ (visited on 05/15/2022).

[16] Makars Šiškins et al. “Sensitive capacitive pressure sensors based on graphene membrane arrays”. en. In: *Microsystems & Nanoengineering* 6.1 (Dec. 2020), p. 102. ISSN: 2055-7434. DOI: 10.1038/s41378-020-00212-3. URL: http://www.nature.com/articles/s41378-020-00212-3 (visited on 12/09/2021).

[17] SeongTak Woo et al. “Realization of a High Sensitivity Microphone for a Hearing Aid Using a Graphene–PMMA Laminated Diaphragm”. In: *ACS Applied Materials & Interfaces* 9.2 (Jan. 2017). Publisher: American Chemical Society, pp. 1237–1246. ISSN: 1944-8244. DOI: 10.1021/acsami.6b12184. URL: https://doi.org/10.1021/acsami.6b12184 (visited on 10/20/2021).

[18] Graham S. Wood et al. “Design and Characterization of a Micro-Fabricated Graphene-Based MEMS Microphone”. In: *IEEE Sensors Journal* 19.17 (Sept. 2019). Conference Name: IEEE Sensors Journal, pp. 7234–7242. ISSN: 1558-1748. DOI: 10.1109/JSEN.2019.2914401.

[19] Sebastian Wittmann et al. “Graphene Membranes for Hall Sensors and Microphones Integrated with CMOS-Compatible Processes”. en. In: *ACS Applied Nano Materials* 2.8 (Aug. 2019), pp. 5079–5085. ISSN: 2574-0970, 2574-0970. DOI: 10.1021/acsanm.9b00998. URL: https://pubs.acs.org/doi/10.1021/acsanm.9b00998 (visited on 10/20/2021).

[20] Roberto Pezone et al. “Sensitive Transfer-Free Wafer-Scale Graphene Microphones”. In: *ACS Applied Materials & Interfaces* (2022).

[21] R. J. Dolleman. “Dynamics of interacting graphene membranes”. en. In: (2018). DOI: 10.4233/uuid:118b4d3e-2d06-4ce7-b5a8-bcc934f0468a. URL: https://repository.tudelft.nl/islandora/object/uuid%3A118b4d3e-2d06-4ce7-b5a8-bcc934f0468a (visited on 04/12/2022).

[22] Minhang Bao and Heng Yang. “Squeeze film air damping in MEMS”. In: *Sensors and Actuators A: Physical* 136.1 (2007), pp. 3–27. ISSN: 0924-4247. DOI: https://doi.org/10.1016/j.sna.2007.01.008. URL: https://www.sciencedirect.com/science/article/pii/S0924424707000118.

[23] Yu Zhou and Farid Amirouche. “Study of fluid damping effects on resonant frequency of an electromagnetically actuated valveless micropump”. en. In: *The International Journal of Advanced Manufacturing Technology* 45.11-12 (Dec. 2009), pp. 1187–1196. ISSN: 0268-3768, 1433-3015. DOI: 10.1007/s00170-009-2053-4. URL: http://link.springer.com/10.1007/s00170-009-2053-4 (visited on 03/21/2022).

[24] Yumei She et al. “The Effect of Viscous Air Damping on an Optically Actuated Multilayer MoS2 Nanomechanical Resonator Using Fabry-Perot Interference”. en. In: *Nanomaterials* 6.9 (Sept. 2016). Number: 9 Publisher: Multidisciplinary Digital Publishing Institute, p. 162. ISSN: 2079-4991. DOI: 10.3390/nano6090162. URL: https://www.mdpi.com/2079-4991/6/9/162 (visited on 04/07/2022).

[25] A. K. Al-mashaal et al. “Dynamic behavior of ultra large graphene-based membranes using electrothermal transduction”. en. In: *Applied Physics Letters* 111.24 (Dec. 2017), p. 243503. ISSN: 0003-6951, 1077-3118. DOI: 10.1063/1.5007327. URL: http://aip.scitation.org/doi/10.1063/1.5007327 (visited on 04/12/2022).

[26] David T. Blackstock. *Fundamentals of Physical Acoustics*. en. Google-Books-ID: e_8sPIEd36YC. John Wiley & Sons, Apr. 2000. ISBN: 978-0-471-31979-5.

[27] Shubham Shubham et al. “A Novel MEMS Capacitive Microphone with Semiconstrained Diaphragm Supported with Center and Peripheral Backplate Protrusions”. In: *Micromachines* 13.1 (2021), p. 22.

[28] Ryan C. Tung, Jason P. Killgore, and Donna C. Hurley. “Liquid contact resonance atomic force microscopy via experimental reconstruction of the hydrodynamic function”. en. In: *Journal of Applied Physics* 115.22 (June 2014), p. 224904. ISSN: 0021-8979, 1089-7550. DOI: 10.1063/1.4882755. URL: http://aip.scitation.org/doi/10.1063/1.4882755 (visited on 03/25/2022).

[29] Moon K. Kwak. “Hydroelastic Vibration of Rectangular Plates”. en. In: *Journal of Applied Mechanics* 63.1 (Mar. 1996), pp. 110–115. ISSN: 0021-8936, 1528-9036. DOI: 10.1115/1.2787184. URL: https://asmedigitalcollection.asme.org/appliedmechanics/article/63/1/110/396399/Hydroelastic-Vibration-of-Rectangular-Plates (visited on 02/07/2023).

[30] M. Amabili, G. Frosali, and M. K. Kwak. “FREE VIBRATIONS OF ANNULAR PLATES COUPLED WITH FLUIDS”. en. In: *Journal of Sound and Vibration* 191.5 (Apr. 1996), pp. 825–846. ISSN: 0022-460X. DOI: 10.1006/jsvi.1996.0158. URL: https://www.sciencedirect.com/science/article/pii/S0022460X96901583 (visited on 10/24/2022).

[31] C.J. Bouwkamp. “A contribution to the theory of acoustic radiation”. In: *Selected Papers on Scalar Wave Diffraction*. Ed. by K.E. Oughstun. SPIE Milestone Series. Bellingham WA, USA: SPIE, 1992, pp. 41–67.

[32] Morse Philip M. *Vibration and Sound*. eng. Mcgraw-hill Book Company, Inc. New York, 1948. URL: http://archive.org/details/dli.ernet.475034 (visited on 08/31/2022).

[33] Brian E Anderson. “Understanding radiation impedance through animations”. In: *Proceedings of Meetings on Acoustics 175ASA*. Vol. 33. 1. Acoustical Society of America. 2018, p. 025003.

[34] M. K. Kwak and K. C. Kim. “Axisymmetric vibration of circular plates in contact with fluid”. en. In: *Journal of Sound and Vibration* 146.3 (May 1991), pp. 381–389. ISSN: 0022-460X. DOI: 10.1016/0022-460X(91)90696-H. URL: https://www.sciencedirect.com/science/article/pii/0022460X9190696H (visited on 10/24/2022).

[35] Jing Xu et al. “Realization of a Graphene/PMMA Acoustic Capacitive Sensor Released by Silicon Dioxide Sacrificial Layer”. en. In: *ACS Applied Materials & Interfaces* 13.32 (Aug. 2021), pp. 38792–38798. ISSN: 1944-8244, 1944-8252. DOI: 10.1021/acsami.1c05424. URL: https://pubs.acs.org/doi/10.1021/acsami.1c05424 (visited on 10/20/2021).

[36] Qin Zhou et al. “Graphene electrostatic microphone and ultrasonic radio”. en. In: *Proceedings of the National Academy of Sciences* 112.29 (July 2015), pp. 8942–8946. ISSN: 0027-8424, 1091-6490. DOI: 10.1073/pnas.1505800112. URL: http://www.pnas.org/lookup/doi/10.1073/pnas.1505800112 (visited on 10/20/2021).

[37] Yu Wu et al. “A Highly Sensitive Fiber-Optic Microphone Based on Graphene Oxide Membrane”. en. In: *Journal of Lightwave Technology* 35.19 (Oct. 2017), pp. 4344–4349. ISSN: 0733-8724, 1558-2213. DOI: 10.1109/JLT.2017.2737639. URL: http://ieeexplore.ieee.org/document/8006203/ (visited on 10/20/2021).

[38] Haslinawati Mohd Mustapha et al. “Characterization of Graphene based Capacitive Microphone”. en. In: *Sains Malaysiana* 48.6 (June 2019), pp. 1201–1207. ISSN: 01266039. DOI: 10.17576/jsm-2019-4806-07. URL: http://www.ukm.my/jsm/pdf_files/SM-PDF-48-6-2019/07%20Haslinawati%20Mohd%20Mustapha.pdf (visited on 10/20/2021).

[39] Jing Xu et al. “Realization of Closed Cavity Resonator Formed by Graphene-PMMA Membrane for Sensing Audio Frequency”. In: *IEEE Sensors Journal* 20.9 (May 2020). Conference Name: IEEE Sensors Journal, pp. 4618–4627. ISSN: 1558-1748. DOI: 10.1109/JSEN.2020.2966415.

[40] Robin J. Dolleman et al. “Graphene Squeeze-Film Pressure Sensors”. en. In: *Nano Letters* 16.1 (Jan. 2016), pp. 568–571. ISSN: 1530-6984, 1530-6992. DOI: 10.1021/acs.nanolett.5b04251. URL: https://pubs.acs.org/doi/10.1021/acs.nanolett.5b04251 (visited on 12/17/2021).

[41] Dejan Davidovikj et al. “Static Capacitive Pressure Sensing Using a Single Graphene Drum”. en. In: *ACS Applied Materials & Interfaces* 9.49 (Dec. 2017), pp. 43205–43210. ISSN: 1944-8244, 1944-8252. DOI: 10.1021/acsami.7b17487. URL: https://pubs.acs.org/doi/10.1021/acsami.7b17487 (visited on 12/08/2021).

[42] Asaad K. Al-mashaal et al. “Tunable Graphene-Polymer Resonators for Audio Frequency Sensing Applications”. In: *IEEE Sensors Journal* 19.2 (Jan. 2019). Conference Name: IEEE Sensors Journal, pp. 465–473. ISSN: 1558-1748. DOI: 10.1109/JSEN.2018.2877463.

[43] J. Scott Bunch et al. “Electromechanical Resonators from Graphene Sheets”. In: *Science* 315.5811 (Jan. 2007). Publisher: American Association for the Advancement of Science, pp. 490–493. DOI: 10.1126/science.1136836. URL: https://www.science.org/doi/full/10.1126/science.1136836 (visited on 04/28/2022).

[44] Arend M. van der Zande et al. “Large-Scale Arrays of Single-Layer Graphene Resonators”. en. In: *Nano Letters* 10.12 (Dec. 2010), pp. 4869–4873. ISSN: 1530-6984, 1530-6992. DOI: 10.1021/nl102713c. URL: https://pubs.acs.org/doi/10.1021/nl102713c (visited on 12/02/2021).

[45] Changyao Chen et al. “Performance of monolayer graphene nanomechanical resonators with electrical readout”. en. In: *Nature Nanotechnology* 4.12 (Dec. 2009), pp. 861–867. ISSN: 1748-3387, 1748-3395. DOI: 10.1038/nnano.2009.267. URL: http://www.nature.com/articles/nnano.2009.267 (visited on 12/02/2021).

[46] Qi Zhang, Daniel Sando, and Valanoor Nagarajan. “Chemical route derived bismuth ferrite thin films and nanomaterials”. In: *Journal of Materials Chemistry C* 4.19 (2016), pp. 4092–4124.

[47] *Polytec laser vibration sensors*. en. URL: https://www.polytec.com/int/vibrometry/products (visited on 02/27/2023).

[48] Shubham Shubham et al. “A Novel MEMS Capacitive Microphone with Semiconstrained Diaphragm Supported with Center and Peripheral Backplate Protrusions”. en. In: *Micromachines* 13.1 (Jan. 2022). Number: 1 Publisher: Multidisciplinary Digital Publishing Institute, p. 22. ISSN: 2072-666X. DOI: 10.3390/mi13010022. URL: https://www.mdpi.com/2072-666X/13/1/22 (visited on 03/23/2022).

[49] Z. Škvor. “On the Acoustical Resistance Due to Viscous Losses in the Air Gap of Electrostatic Transducers”. In: *Acta Acustica united with Acustica* 19.5 (Jan. 1967), pp. 295–299.

[50] Robin J. Dolleman et al. “Squeeze-Film Effect on Atomically Thin Resonators in the High-Pressure Limit”. en. In: *Nano Letters* 21.18 (Sept. 2021), pp. 7617–7624. ISSN: 1530-6984, 1530-6992. DOI: 10.1021/acs.nanolett.1c02237. URL: https://pubs.acs.org/doi/10.1021/acs.nanolett.1c02237 (visited on 03/16/2022).

[51] Tung Shen Chew. “Avoiding Epic Fails in MEMS Microphones”. en. In: (2017), p. 13.

[52] Altti Torkkeli et al. “Capacitive microphone with low-stress polysilicon membrane and high-stress polysilicon backplate”. In: *Sensors and Actuators A: Physical* 85.1 (2000), pp. 116–123. ISSN: 0924-4247. DOI: https://doi.org/10.1016/S0924-4247(00)00336-8. URL: https://www.sciencedirect.com/science/article/pii/S0924424700003368.